

Recent Advances in Stabilization of Sodium Metal Anode in Contact with Organic Liquid and Solid-State Electrolytes

Qiongqiong Lu,* Aikai Yang, Ahmad Omar, Qianli Ma, Frank Tietz, Olivier Guillon, and Daria Mikhailova*

Sodium (Na) metal is considered as the promising anode for next-generation high-energy-density Na-metal batteries owing to its highest specific capacity and lowest electrochemical potential among all Na-based anode candidates. However, the Na metal anode suffers from considerable volume change, nonuniform Na deposition, and an unstable electrode–electrolyte interface, which result in rapid capacity fade and poor cycling stability, hampering its practical application. To tackle aforementioned issues, many strategies have been developed to accommodate and guide Na nucleation/growth as well as stabilize the interface, including structure stabilization by applying 3D host materials, electrolyte modification and interface engineering to form stable interfaces and guide the Na deposition, etc. The present review is intended as a guideline through the fundamental challenges affecting the performance of Na metal anodes along with corresponding mitigation strategies. Moreover, the specific mechanisms for stabilizing Na metal anodes are discussed in detail. Apart from the stabilization of the Na metal anode in contact with liquid electrolytes, attention has also been paid to the review of stabilization of the Na metal anode in contact with solid-state electrolytes. Furthermore, unresolved challenges and promising perspectives for stable Na metal anodes in practical applications are presented.

1. Introduction


The continuous usage of fossil fuels has resulted in a severe climate change leading to global warming. It is very important and urgent to reduce CO₂ emissions through a significantly large improvement in the utilization of fluctuating energy sources such as solar energy, wind energy, etc.^[1] However, the intermittent energy sources require the energy storage systems to balance the energy demands. The most widespread energy storage system lithium-ion batteries (LIBs) have been widely used for consumer electronics in daily life due to their high energy density and long cycle life.^[2] However, the state-of-the-art LIBs cannot meet the increasing demand of batteries with low cost for the large-scale stationary energy storage systems due to the uneven geological distribution of lithium and dramatically rising costs over time.^[3] Therefore, there is a strong effort toward the development of alternative chemistries based on other naturally abundant cations such as sodium ions.^[4,5]

Sodium-ion batteries (SIBs) provide a promising alternative choice for LIBs due to high abundance of sodium resources and the potential low cost,^[6–8] while the practical application of SIBs is hindered by some significant challenges. As the electrochemical performance of batteries mainly relies on the electrode materials, designing electrode materials with high performance is essential for accelerating viable applications of SIBs.^[9,10] Among the anode materials, carbon-based materials have a low cost, but they provide low specific capacities.^[11] In addition, graphite as a widely used anode material for commercial LIBs shows a failed application in SIBs. Although many metallic alloys possess high electronic conductivity and have a high theoretical specific capacity, they suffer from large volume change during insertion and extraction of the alkali metal ions.^[12] Transition metal oxides/sulfides also possess high theoretical specific capacity, but they face an additional problem of low conductivity along with huge volume change.^[13] Sodium metal is a promising anode for SIBs owing to its high theoretical specific capacity (1166 mAh g^{−1}), low redox potential (−2.714 V vs the standard hydrogen electrode), natural abundance, and potential low cost. However, there are significant scientific and practical challenges, including volume change, unstable solid–electrolyte

Q. Lu, A. Omar, D. Mikhailova
Institute of Complex Materials
Leibniz Institute for Solid State and Materials Research (IFW) Dresden e.V.
Helmholtzstr. 20, 01069 Dresden, Germany
E-mail: q.lu@ifw-dresden.de; d.mikhailova@ifw-dresden.de

A. Yang, Q. Ma, F. Tietz, O. Guillon
Institute of Energy and Climate Research
Materials Synthesis and Processing (IEK-1)
Forschungszentrum Jülich GmbH
52425 Jülich, Germany

A. Yang, O. Guillon
Institute of Mineral Engineering
Rheinisch-Westfälische Technische Hochschule (RWTH) Aachen
University
Mauerstraße 5, 52064 Aachen, Germany

 The ORCID identification number(s) for the author(s) of this article can be found under <https://doi.org/10.1002/ente.202200149>.

© 2022 The Authors. Energy Technology published by Wiley-VCH GmbH. This is an open access article under the terms of the Creative Commons Attribution-NonCommercial-NoDerivs License, which permits use and distribution in any medium, provided the original work is properly cited, the use is non-commercial and no modifications or adaptations are made.

DOI: 10.1002/ente.202200149

interphase (SEI), dendrite formation, and gas evolution, which need to be overcome for the implementation of the Na metal anode toward applications in Na-metal batteries (SMBs).^[14]

This review provides the fundamental challenges of Na metal anodes in contact with organic liquid and solid-state electrolytes (SSEs) along with progressive solution strategies. The mechanisms of strategies for stabilizing Na metal anodes are discussed in detail. Furthermore, the high reactivity of Na metal is accompanied by the gas evolution behavior to some extent in the liquid electrolyte battery system.

2. Major Challenges of Na Metal Anode

Na metal anode has similar issues in batteries with both organic liquid electrolytes and SSEs, such as structural change, unstable electrode | electrolyte interface, and formation of Na metal dendrites. Furthermore, the high reactivity of Na metal is accompanied by the gas evolution behavior to some extent in the liquid electrolyte battery system.

2.1. Challenges of Na Metal in Contact with Liquid Electrolyte

2.1.1. Structural Change

The bulk or so-called “hostless” Na metal anode undergoes a large volume change in the process of plating and stripping during the operation of SMBs. In the stripping process, as a large amount of Na metal is oxidized to Na ions and dissolved in the electrolyte, the volume of Na metal anode dramatically decreases. In the following plating process, Na ions are reduced to Na metal and are deposited on the electrode or current collector, thus increasing the electrode volume. In addition, Na metal tends to deposit in branch-like morphologies. The deposited Na with a highly loose structure and huge surface area aggravates the volume change and chemical reactions between the Na metal and electrolytes. Such drastic volume variation and uncontrollable side reactions result in poor mechanical stability and a poor electrochemical stability of the Na anode.^[15,16]

2.1.2. Unstable Interface

As the chemical potential of Na metal is located above the lowest unoccupied molecular orbital (LUMO) of most organic electrolytes, Na reacts with the electrolytes forming a SEI, which is composed of both inorganic components (e.g., NaF, Na₂CO₃, etc.) and organic components (e.g., ROCO₂Na, HCOONa, etc.).^[17] It was reported that inorganic components are located in the internal layer of the SEI, while organic components are lying on the external layer of SEI, which is similar to those of the Li metal anode. The SEI normally shows a thickness of hundreds of nanometers with a mosaic structure.^[18,19] A desired SEI should possess a high conductivity of Na⁺ cations and poor electronic conductivity, which can prevent further decomposition of electrolytes, suppress the dendrite growth, and minimize the volume change. The chemically and morphologically heterogeneous SEI formed on the Na metal anode is unstable and evolves in both structure and chemical composition during cycling. Specifically, the SEI is not mechanically robust and flexible enough to withstand the tremendous strain induced by Na

dendrites and the drastic volume change of the Na metal anode.^[20,21] Therefore, repeated Na stripping/plating would lead to cracks, and consequently, fresh and unprotected metallic Na is exposed at broken regions of the SEI, where it reacts with the electrolyte to form a new SEI. The reaction is irreversible and continuously consumes Na and electrolyte, thus leading to a capacity fade. Besides, Na⁺ ions preferentially deposit at the broken SEI regions due to more favorable thermodynamics and faster kinetics, aggravating a nonuniform Na plating behavior and dendrite formation.^[22,23]

2.1.3. Na Dendrite Formation

Several theories have been proposed to explain the driving forces for Li or Na dendrite growth in liquid organic electrolytes, including the nucleation theory,^[24] space charge theory,^[25] nonuniform charge distribution theory,^[26] stress-induced theory,^[27] spherical diffusion theory,^[28] etc. Among these, the nucleation theory and space charge theory have been experimentally verified.^[24,29]

According to thermodynamics, there is an energy barrier for the nucleation of a critical cluster of Na atoms (Figure 1a).^[30] Na nuclei can be described as spherical particles with a radius r and contact angle θ to the substrate. The Gibbs energy of nucleation process ($\Delta G_{\text{nucleation}}$) can be described as the sum of its bulk free energy and surface free energy

$$\Delta G_{\text{nucleation}} = -\frac{4}{3}\pi r^3 \Delta G_v + 4\pi r^2 \gamma_{\text{NE}} \quad (1)$$

where ΔG_v and γ_{NE} represent the free energy change per volume and the surface energy of the Na nuclei|electrolyte interface, respectively. The relationship between the deposition overpotential η and ΔG_v can be described by the following equation

$$\Delta G_v = \frac{F|\eta|}{V_m} \quad (2)$$

where F and V_m represent Faraday's constant and molar volume of Na, respectively. The value of $\Delta G_{\text{nucleation}}$ reaches zero as nucleation takes place. Thus, the critical radius is determined by the following formula^[32]

$$r_{\text{critical}} = \frac{2\gamma V_m}{F|\eta|} \quad (3)$$

and the nuclei size is inversely proportional to the overpotential. Typically, there are two important characteristic overpotentials observed during Na electrodeposition: the nucleation overpotential (η_n) and the plating overpotential (η_p) (Figure 1b). At the beginning of the Na deposition process, the potential decreases to $-\eta_n$ at which the nucleation of Na grains occurs. After initial nucleation, the overpotential increases to $-\eta_p$ at which Na nuclei grow. Because η_p is lower as compared to η_n , the accumulation of Na atoms on existing Na nuclei is more favorable than the formation of new stable Na clusters due to a lower energy barrier.^[33,34]

As the overpotential is proportional to the applied current density and number density of nuclei is proportional to the cubic power of overpotential, the deposited Na particles are relatively large and sparsely dispersed at a low current density, while the deposited Na shows much more nuclei and a wide spread tight morphology at high current density.^[24]

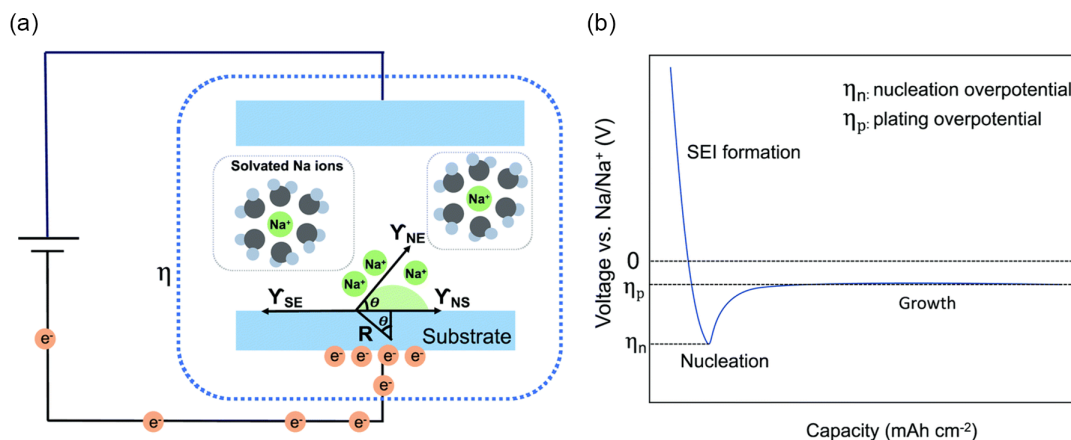


Figure 1. a) Schematic of Na heterogeneous nucleation on a substrate. b) Schematic illustration of a typical voltage profile of Na deposition. Reproduced with permission.^[31] Copyright 2020, Royal Society of Chemistry.

Actually, the heterogeneous nucleation of Na is also influenced by properties of the substrate, which are reflected in the contact angle. In addition, the contact angle θ can be written as the following equation

$$\cos \theta = \frac{\gamma_{SE} - \gamma_{NS}}{\gamma_{NE}} \quad (4)$$

where γ_{SE} , γ_{NS} , and γ_{NE} refer to the surface energy of solid substrate, surface energy of Na nuclei, and surface energy of interface of Na nuclei–electrolyte, respectively.

If a reaction occurs during the nucleation process, the change in Gibbs free energy of the reaction (ΔG_r) can also contribute to the spreading of molten Na, resulting in a smaller contact angle.

$$\cos \theta_r = \cos \theta - \frac{\Delta \gamma_{SE} + \Delta G_r}{\gamma_{NE}} \quad (5)$$

where θ_r is the contact angle after reaction, and $\Delta \gamma_{SE}$ stands for the change in the interface energy between the substrate and electrolyte due to a new interphase formation. Accordingly, a more negative ΔG_r value and a decrease in γ_{SE} can lead to a small contact angle, and, therefore, to a better wettability (Figure 2). Alternatively, the adsorption reaction on the surface corresponds to the binding energy between Na and the substrate. Hence, a high binding energy can lead to a good wettability. Therefore,

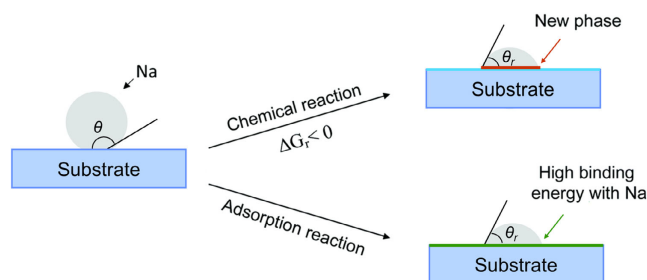


Figure 2. Schematic illustration of the interface properties on Na wettability. Reproduced with permission.^[31] Copyright 2020, Royal Society of Chemistry.

the most common method for tuning the surface energy is a surface treatment, including thin film coating and implantation of nano/microscale species that can react with the Na metal or possess high binding energy to the Na metal.

Although the nucleation theory can explain the initial nucleation process, it is not suitable for the particle growth after nucleation.

The space charge theory predicts when the condition

$$\frac{dC}{dx} > 2C_0/L \quad (6)$$

is satisfied^[25] (with C_0 as the initial concentration of Na ions, L the distance between the cathode and anode) that a Na dendrite would evolve at the time τ , called the “Sand’s time”

$$\tau = \pi D \left(\frac{C_0 e}{2J t_a} \right)^2 \quad (7)$$

$$t_a = 1 - t_{Na^+} = \frac{\mu_a}{\mu_a + \mu_{Na^+}} \quad (8)$$

where D is the diffusion coefficient, e is the electron charge, J is the effective current density for the electrode, t_a , t_{Na^+} and μ_a , μ_{Na^+} are the transference numbers and mobility of anions and Na ions, respectively.^[25] Therefore, decreasing the effective current density by increasing the electrode surface area and/or by improving the mobility of Na⁺ ions is essential for prolonging the Sand’s time and thus delaying Na dendrite formation.

2.1.4. Gas Evolution

Additionally, owing to the high reactivity of Na toward the organic components of the electrolyte, the evolution of flammable gases causes severe safety hazards. Dugas et al.^[35] investigated gas evolution in the system composed of Na in 1 M NaPF₆ in EC/DMC (v:v 1:1) without and with 3% FEC. The CO₂ and CO have been detected by GC/FTIR after soaking Na in 1 M NaPF₆ in EC/DMC (v:v 1:1) for 5 d, while the amount of CO₂ and CO became larger and additionally CH₄ and C₂H₄ were generated after 48 d. When using the electrolyte with 3%

FEC, only CO₂ gas was detected, which amount increased between 5 and 48 d. The emission was 120 μmol cm⁻² for electrolyte without FEC, while it was 20 μmol cm⁻² for electrolyte with 3% FEC. Chen et al.^[36] found out that the LUMO of the ion–solvent complex [(NaX)⁺, X = propylene carbonate (PC), tetraethylene glycol dimethyl ether (TEGDME), 1,2-dimethoxyethane (DME)] facilitated the gas evolution, which was verified by *in situ* optical microscopy combined with first-principles calculations. Besides, the impact of sodium salts (such as sodium trifluoromethanesulfonate (NaOTf), sodium bis(fluorosulfonyl)imide (NaFSI), sodium bis(trifluoromethanesulfonyl)imide (NaTFSI), NaClO₄, and NaPF₆) on gas evolution in symmetric cells was investigated by Goktas et al., and diglyme was used as solvent.^[37] The amount of gas evolution (H₂, CH₄, CO, and C₂H₄) was quantified by online mass spectroscopy.

2.2. Challenges of Na Metal Anode in Solid-State Batteries

2.2.1. Structural Change

The deposition of Na metal poses even more severe volume change problem in anode-free batteries and solid-state batteries (SSBs). In anode-free batteries, Na⁺ ions from the cathode are deposited on the anode side, leading to an inevitable volume change. In SSBs, especially with inorganic SSEs, the volume change and good contact between the Na metal and the SSE is difficult to guarantee during repeated stripping/plating due to its rigid properties and typical operation under considerable pressure, which can deteriorate the interface and thus increase the polarization resistance of the cell.^[38]

2.2.2. Unstable Interface

In SSBs, the solid–solid interface between Na metal and SSE remains a considerable challenge for the development of practical batteries. The high reactivity of metallic Na also results in a reduction of the SSEs, thus destabilizing the Na–electrolyte interface and deteriorating the electrochemical performance.^[39] For example, the Na₃PS₄ electrolyte decomposes into poorly ionically conducting and electronically insulating interlayer composed of sodium sulfide and sodium phosphide when it contacts to the Na metal.^[40] In addition, volume changes upon plating and stripping (i.e., charge and discharge) of the Na metal electrode further result in a rather unstable interface between Na and SSE. The intimate contact between Na metal and SSE with high ionic conductivity and chemical/electrochemical stability can reduce the interfacial impedance, which can be evaluated in terms of area-specific resistance (ASR), and ensure a homogeneous stripping/plating of Na⁺ ions. The calculation of ASR of the interface between Na metal and SSE can be written as Equation (9)

$$\text{ASR} = R_{\text{inter}} S \quad (9)$$

where R_{inter} indicates the interfacial resistance derived from the internal resistance of the cell and S indicates the effective contact area between Na and SSE. In the case, the contact area of both sides is involved like in the symmetric cells with Na metal as electrodes, and then the measured R_{inter} has to be divided by 2.

A high ASR gives rise to a high overpotential, which can reduce the overall energy efficiency of the cell, and triggers an inhomogeneous nucleation in the Na⁺ ion plating process, in turn increasing the local current density and inducing formation of dendrites.

An interface can be artificially modified by additional layers to achieve a good interfacial contact between Na and SSE while reducing the interfacial impedance and enhancing the critical current density (CCD, depicted as J_c), which is a further common parameter to evaluate the performances of the SSE and the interfacial contact between Na and SSE. The CCD is defined as the transport current at which the flow voltage (e.g., significant voltage drift) clearly appears. The CCD is given by the critical current I_c divided by the cross-sectional area S of the contact region, as described in Equation (10)

$$J_c = \frac{I_c}{S} \quad (10)$$

In the CCD measurement, the polarization voltage is relatively smooth before reaching the CCD; when CCD is reached, there is a significant fluctuation in the polarization voltage, followed by short circuit. The CCD depends on the properties of the SSE material itself and the stability of the interface between the Na metal and the SSE.

2.2.3. Na Dendrite Formation

In SSBs, the sluggish replenishment rate of Na⁺ ions due to intrinsic low self-diffusion during in the Na metal stripping unavoidably leads to the interface deterioration that destroys the initial physical contact by forming interfacial voids and triggering the dendrite growth (Figure 3a). During stripping, the Na metal atoms will produce equivalent vacancies, which will accumulate into voids due to high stripping rate (i.e., high current density). The consumed flux of Na atom (J_{consume}) is proportional to the applied current (i) and inversely proportional to the effective reaction area (A_{eff}), as it can be expressed by Equation (11).^[41–43] Meanwhile, the creep and diffusion of the Na will prompt the Na atoms to replenish the vacancies, where the replenished Na atom flux ($J_{\text{replenish}}$) can be expressed as in Equation (12)

$$J_{\text{consume}} = \frac{i}{A_{\text{eff}} \times e} \quad (11)$$

$$J_{\text{replenish}} = J_{\text{creep}} + J_{\text{diffusion}} \quad (12)$$

The creep rate (J_{creep}) and diffusion rate ($J_{\text{diffusion}}$) mainly relate to the intrinsic properties of Na metal and the external pressure and temperature.^[45] 1) When $J_{\text{consume}} > J_{\text{replenish}}$, the consumption rate of Na atoms is faster than the rate at which it can be replenished; vacancies accumulate at the interface to form voids and lead to the deterioration of the interface. The contact loss caused by these formed voids can be remedied by applying external pressure in consideration of the elastic and plastic deformation of Na metal and SSE by annihilating the produced pores^[44]; and 2) When $J_{\text{consume}} \leq J_{\text{replenish}}$, the rate of sodium atoms replenishing vacancies is fast enough that the interface

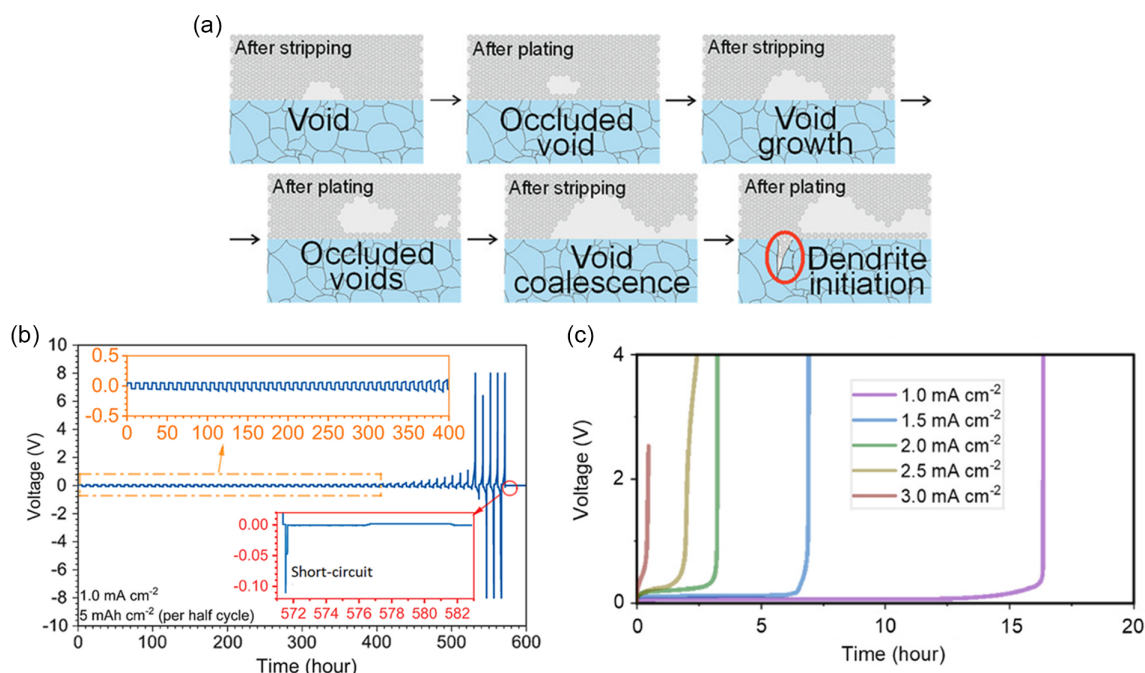


Figure 3. a) Schematic of Na metal|SSE interface. Reproduced with permission.^[44] Copyright 2020, American Chemical Society. b) Galvanostatic cycling of a Na/NZSP/Na symmetric cell at 1.0 mA cm^{-2} , 5 mAh cm^{-2} (per half cycle) at 25°C . Partially enlarged plots are also shown as insets. c) DC polarization experiments on Na/NZSP/Na symmetric cells at 25°C . Reproduced with permission.^[45] Copyright 2020, Elsevier.

remains stable without voids during sodium stripping, which is desired.^[46]

The Na|SSE interface exhibits formation of voids in the Na anode at the interface during stripping, which accumulate on cycling leading to increasing interfacial current density and induce dendrites on plating, short circuit, and hence cell failure.^[44] Tsai et al.^[45] experimentally verified that long-term charging or cycling will destroy the interface between Na and SSE with CCD measurement and comparison of different capacities (Figure 3b,c). Recently, Sun et al.^[47] proposed another mechanism of capacity fading for Na-SSBs revealed by synchrotron X-Ray tomography caused by electrochemically generated inactive Na electrodeposits. In addition, the space charge model is widely adopted to describe the persistent growth of dendrite, which proposes that the formed voids in the metal lead to enrichment of regional space charge, thus an enriched electric field forms and then the dendritic growth occurs.^[48]

3. Strategies for Sodium Metal Stabilization

Even though Na and Li show similar properties due to the same alkali metal group, the Na metal anode does not face exactly the same scientific challenges as compared with the Li metal. Na possesses a higher chemical reactivity due to the lower first ionization energy ($498.8 \text{ kJ mol}^{-1}$) as compared with that of Li ($520.2 \text{ kJ mol}^{-1}$).^[49] The more reactive Na easily reacts with traditional carbonate-based electrolytes forming nonuniform SEI composed of inorganic Na salts and polymers on the Na metal surface. The inorganic Na salts are prone to dissolve in the electrolyte due to the weaker Lewis acid nature of Na^+ leading to

unstable SEI.^[50] On the other hand, the weaker Lewis acid nature of Na^+ is beneficial for ionic transport, facilitating Na^+ deposition.^[51] In addition, the deposited Na with an extremely soft and fragile nature as well as mossy morphology is prone to break and form nonactive Na, leading to a failure of SMBs when excess electrolyte is used.^[52] The reaction between electrolytes and deposited mossy Na induces the continuous consumption of electrolytes, thus the depletion of electrolytes would happen when a limited electrolyte amount is used. This is different from the failure of Li-metal batteries mostly induced by dendrite. Owing to the abovementioned different electrochemical behavior between Li and Na metal, the efficacy of strategies for Li metal on stabilization of Na is unguaranteed and needs to be additionally studied in detail.

3.1. Sodium Metal Stabilization in Liquid Electrolytes

In order to address the challenges of the sodium metal anode in batteries with liquid electrolytes, solutions including structure stabilization, electrolyte optimization, and interface engineering have been developed. The summary of various methods for stabilizing Na metal anode in SMBs with organic liquid electrolytes is listed in Table 1.

3.1.1. Structure Stabilization

To address the volume expansion of Na metal anodes, a host materials with a porous structure are essential to provide space for accommodating plated Na.^[80,81] In particular, 3D conductive hosts with a high surface area can reduce the effective current

Table 1. Comparison of performance of SMBs with organic liquid electrolytes.

Strategy	Electrolyte	Coulombic efficiency	Lifespan in symmetric cells	Full cells performance	References
Electrochemical plating Na into CuNW-Cu	1 M NaPF ₆ in DME	99.7% for 1400 h at 1 mA cm ⁻² with 2 mAh cm ⁻²	20 mV after 500 h at 1 mA cm ⁻² with 1 mAh cm ⁻²	Coupled with FeS ₂ , 286 mAh g ⁻¹ at 1 A g ⁻¹ , 320 mAh g ⁻¹ after 50 cycles at 0.2 A g ⁻¹	[53]
Electrochemical plating Na into porous Al	1 M NaPF ₆ in diglyme	99.8% for 1000 h at 1 mA cm ⁻² with 0.5 mAh cm ⁻²	16 mV after 1000 h at 0.5 mA cm ⁻² with 0.25 mAh cm ⁻²	In Na–O ₂ full cell, 600 mAh g ⁻¹ after 200 cycles at 0.1 mA cm ⁻²	[54]
Mechanical rolling Na into 3D Ni foam	1 M NaPF ₆ in diglyme	–	13 mV after 600 h at 1 mA cm ⁻² with 1 mAh cm ⁻²	Coupled with Na ₃ V ₂ (PO ₄) ₃ , 76 mAh g ⁻¹ at 2 C, 75 mAh g ⁻¹ after 200 cycles at 1 C (1 C = 118 mA g ⁻¹)	[55]
Molten Na infusion into carbon felt	1 M NaClO ₄ in EC/PC (v/v = 1:1)	–	20 mV after 480 h at 1 mA cm ⁻² with 2 mAh cm ⁻²	Coupled with Na _{0.67} Ni _{0.33} Mn _{0.67} O ₂ , 30 mAh g ⁻¹ at 4 C, 72 mAh g ⁻¹ after 200 cycles at 1 C (1 C = 80 mA g ⁻¹)	[56]
Electrochemical plating Na into 1 M NaClO ₄ in EC/DEC carbonized wood	(v/v = 1:1)	–	≈30 mV after 250 h at 0.5 mA cm ⁻² with 0.25 mAh cm ⁻²	–	[15]
Electrochemical plating Na into O-containing carbonized coconut framework	1 M NaPF ₆ in diglyme	99.6% for 2000 h at 5 mA cm ⁻² with 10 mAh cm ⁻²	≈ 5.3 mV after 700 h at 10 mA cm ⁻² with 1 mAh cm ⁻²	Coupled with Na ₃ V ₂ (PO ₄) ₃ , 107 mAh g ⁻¹ after 100 cycles at 0.4 C (1 C = 118 mA g ⁻¹)	[57]
Molten Na infusion into reduced graphene oxide (rGO)	1 M NaPF ₆ in diglyme	–	≈15 mV after 600 h at 1 mA cm ⁻² with 1 mAh cm ⁻²	Coupled with Na ₃ V ₂ (PO ₄) ₃ , 105 mAh g ⁻¹ at 2 C, 90 mAh g ⁻¹ after 100 cycles at 1 C (1 C = 118 mA g ⁻¹)	[58]
Electrochemical plating Na into N-doped mesoporous carbon	1.5 M NaSO ₃ CF ₃ in diglyme	97% for 750 h at 1 mA cm ⁻² with 8 mAh cm ⁻²	≈19 mV after 1000 h at 1 mA cm ⁻² with 1 mAh cm ⁻²	–	[59]
Electrochemical plating Na into N,O-doped graphitized carbon fibers	1 M NaPF ₆ in diglyme	99.9% for 1600 h at 1 mA cm ⁻² with 8 mAh cm ⁻²	≈30 mV after 1238 h at 2 mA cm ⁻² with 1 mAh cm ⁻²	Coupled with Na ₃ V ₂ (PO ₄) ₃ , 95 mAh g ⁻¹ after 80 cycles at 0.5 C (1 C = 118 mA g ⁻¹)	[60]
Molten Na infusion in Fe ₂ O ₃ coated carbon textile	1 M NaClO ₄ in EC/DEC (v/v = 1:1)	–	≈20 mV after 333 h at 1 mA cm ⁻² with 1 mAh cm ⁻²	–	[61]
Molten Na infusion in SnO ₂ grown on carbon textile	1 M NaClO ₄ in EC/DMC (v/v = 1:1)	–	≈50 mV after 220 h at 1 mA cm ⁻² with 1 mAh cm ⁻²	–	[62]
Carbon paper interlayer	1 M NaSO ₃ CF ₃ in diglyme	–	≈60 mV after 480 h at 5 mA cm ⁻² with 1 mAh cm ⁻²	Coupled with Na ₃ V ₂ (PO ₄) ₃ , 105 mAh g ⁻¹ at 4 C, 100 mAh g ⁻¹ after 36 cycles at 0.1 C (1 C = 118 mA g ⁻¹)	[63]
N,S-doped carbon nanotube interlayer	1 M NaSO ₃ CF ₃ in diglyme	99.8% for 400 h at 1 mA cm ⁻² with 1 mAh cm ⁻²	≈30 mV after 500 h at 1 mA cm ⁻² with 1 mAh cm ⁻²	In Na–O ₂ full cell, stable cycling 90 cycles at 0.1 mA cm ⁻² with a capacity limit of 0.5 mAh cm ⁻²	[64]
Gradient Ag coated CNT film as interlayer	1 M NaPF ₆ in diglyme	99.5~99.9% for 800 h at 1 mA cm ⁻² with 4 mAh cm ⁻²	≈200 mV after 1000 h at 8 mA cm ⁻² with 8 mAh cm ⁻²	Coupled with Na ₃ V ₂ (PO ₄) ₃ , 75 mAh g ⁻¹ after 500 cycles at 2 C (1 C = 118 mA g ⁻¹)	[65]
Electrochemical plating Na on C@Sb nanoparticle as nucleation layer on Cu foil	1 M NaSO ₃ CF ₃ in diglyme	99.75% for 1800 h at 1 mA cm ⁻² with 1 mAh cm ⁻²	≈31 mV after 2400 h at 1 mA cm ⁻² with 1 mAh cm ⁻²	Coupled with Na ₃ V ₂ (PO ₄) ₃ , 89 mAh g ⁻¹ after 500 cycles at 1 C (1 C = 117 mA g ⁻¹)	[66]
Ether electrolytes	1 M NaPF ₆ in diglyme	99.9% for 1200 h at 0.5 mA cm ⁻² with 1 mAh cm ⁻²	–	–	[67]
High-concentration electrolyte	4 M NaN(FSO ₂) ₂ in DME	99% for 600 h at 1 mA cm ⁻² with 1 mAh cm ⁻²	–	Coupled with Na ₃ V ₂ (PO ₄) ₃ , 75 mAh g ⁻¹ at 4 C, 100 mAh g ⁻¹ after 100 cycles at 0.5 C (1 C = 120 mA g ⁻¹)	[68]

Table 1. Continued.

Strategy	Electrolyte	Coulombic efficiency	Lifespan in symmetric cells	Full cells performance	References
Localized high-concentration electrolytes	2.1 M NaN(FSO ₂) ₂ in DME:BTFE (molar ratio 1:2)	98.95% for 800 h at 1 mA cm ⁻² with 1 mAh cm ⁻²	≈ 25 mV after 2000 h at 1 mA cm ⁻² with 1 mAh cm ⁻²	Coupled with Na ₃ V ₂ (PO ₄) ₃ , 92 mAh g ⁻¹ at 1 °C, 66.4 mA h g ⁻¹ after 40 000 cycles at 2 °C (1 C = 120 mA g ⁻¹)	[63]
NaF coating on Na metal prepared by fluoroethylene carbonate pretreatment	1 M NaCF ₃ SO ₃ in tetraglyme	–	≈ 100 mV after 250 h at 0.15 mA cm ⁻² with 0.075 mAh cm ⁻²	In Na–O ₂ full cell, stable cycling 50 cycles at 0.25 mA cm ⁻² with a capacity limit of 1000 mAh g ⁻¹	[69]
Na–Sn alloy/NaCl coating on Na metal by using SnCl ₂ as additive	1 M NaClO ₄ in EC/PC (v/v = 1:1)	–	≈ 50 mV after 500 h at 0.5 mA cm ⁻² with 1 mAh cm ⁻²	Coupled with Na ₃ V ₂ (PO ₄) ₃ , 101 mAh g ⁻¹ at 1 °C, 100 mA h g ⁻¹ after 250 cycles at 1 C	[70]
KTFSI as additive using shield effect	1 M Na CF ₃ SO ₃ in tetraglyme	98.3% for 560 h at 1 mA cm ⁻² with 1 mAh cm ⁻²	≈ 14 mV after 2700 h at 1 mA cm ⁻² with 1 mAh cm ⁻²	–	[71]
Al ₂ O ₃ coating on Na metal surface by low-temperature plasma-enhanced ALD	1 M NaClO ₄ in EC/DEC (v/v = 1:1)	–	≈ 70 mV after 400 h at 0.25 mA cm ⁻² with 0.075 mAh cm ⁻²	–	[72]
Al ₂ O ₃ coating on Na metal by ALD	1 M NaSO ₃ CF ₃ in diglyme	–	≈ 20 mV after 500 h at 1 mA cm ⁻² with 3 mAh cm ⁻²	–	[73]
Na–MoS ₂ composite anode	1 M NaClO ₄ in EC/DEC (v/v = 1:1) with 10% FEC	–	≈ 15 mV after 100 h at 0.5 mA cm ⁻² with 0.25 mAh cm ⁻²	Coupled with Na ₃ V ₂ (PO ₄) ₃ , 50 mAh g ⁻¹ at 6C, 100 mAh g ⁻¹ after 100 cycles at 1 C (1 C = 118 mA g ⁻¹)	[74]
Graphene film protection layer on Na metal	1 M NaPF ₆ in EC/DEC (v/v = 1:1)	–	≈ 250 mV after 200 h at 1 mA cm ⁻² with 1 mAh cm ⁻²	–	[74]
Electropolymerized ionic liquids on Na metal	1 M NaClO ₄ in EC/PC (v/v = 1:1)	–	≈ 35 mV after 40 h at 1 mA cm ⁻² with 1 mAh cm ⁻²	Coupled with Na ₃ V ₂ (PO ₄) ₃ , 97 mAh g ⁻¹ after 160 cycles at 100 mA g ⁻¹	[75]
Al ₂ O ₃ /PVDF-HFP coating by blast casting	1 M NaClO ₄ in EC/PC (v/v = 1:1)	–	≈ 1000 mV after 550 h at 0.5 mA cm ⁻² with 1 mAh cm ⁻²	Coupled with Na _{0.6} Mn _{0.65} Ni _{0.25} Co _{0.10} O ₂ , 93 mAh g ⁻¹ after 60 cycles at 0.5 C	[76]
NaBr coating on Na metal by 1-bromopropane treatment	1 M NaPF ₆ EC/PC (v/v = 1:1)	–	≈ 150 mV after 250 h at 1 mA cm ⁻² with 1 mAh cm ⁻²	Coupled with sulfur-PAN, 400 mAh g ⁻¹ after 250 cycles	[77]
Bi coating on Na metal by Bi(SO ₃ CF ₃) ₃ -DME solution treatment	1 M NaSO ₃ CF ₃ in diglyme	–	≈ 25 mV after 1000 h at 0.5 mA cm ⁻² with 1 mAh cm ⁻²	In Na–O ₂ full cell, stable cycling 50 cycles at 0.15 mA cm ⁻² with a capacity limit of 1000 mAh g ⁻¹	[78]
Poly(DOL) coating on Na metal by DOL pretreatment	1 M NaPF ₆ in tetraglyme	–	≈ 25 mV after 2800 h at 1 mA cm ⁻² with 1 mAh cm ⁻²	Coupled with Na ₃ V ₂ (PO ₄) ₃ , 80 mAh g ⁻¹ at 5 C, 94 mAh g ⁻¹ after 200 cycles at 0.5 C (1 C = 118 mA g ⁻¹)	[79]

density, which will delay the dendrite formation according to the “Sand's time” model and prolong the battery cycle life. Hosts with sodiophilic sites not only can improve the wettability toward molten Na facilitating the large-scale fabrication of Na composite using facile molten Na infusion method, but also can guide uniform Na nucleation suppressing a Na dendrite growth.^[82] Wang et al.^[53] fabricated in situ grown Cu nanowires on 3D Cu foam (CuNW-Cu) as a host for Na plating/stripping. The increasing surface area enabled a reduced local current density and offered abundant nucleation sites, resulting in homogeneous Na deposition. Consequently, the Na metal anode can operate for more than 1400 h on CuNW-Cu with a low overpotential and a thickness variation of 2% at a current density of 1.0 mA cm⁻² with

2.0 mAh cm⁻² capacity. Furthermore, porous Al with reduced cost and lower weight than Cu was employed as a substrate for Na plating.^[54] The surface for Na nucleation and deposition was increased, and Na⁺ flux distribution was reduced due to the interconnected porous structure of Al, resulting in a uniform Na nucleation and deposition (**Figure 4a**). As a result, a stable cycling over 1000 h at 0.5 mA cm⁻² was obtained in symmetric cells with help of the porous Al current collector. Besides, Lu et al.^[55] applied 3D Ni foam as Na host and 3D Ni/Na hybrid anode was fabricated by mechanical rolling process. They found out that the 3D Ni/Na showed a lower overpotential in symmetric cell, while superior capacity was obtained in full cells paired with a Na₃V₂(PO₄)₃ cathode, owing to the suppressed volume change

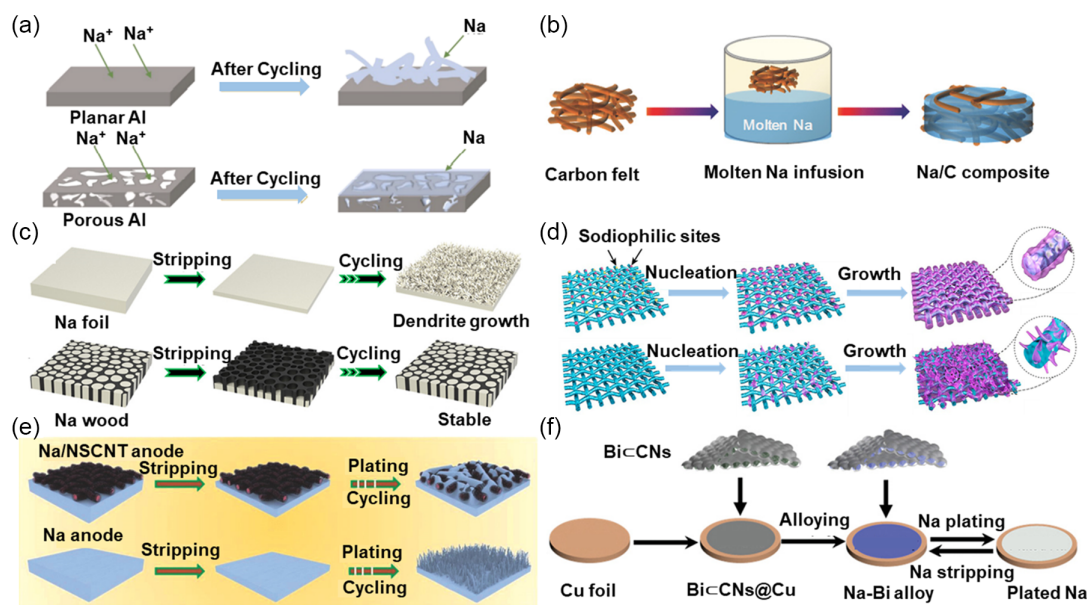


Figure 4. a) Schematic of Na deposition behavior on planar and porous Al foils. Reproduced with permission.^[54] Copyright 2017, American Chemical Society. b) Schematic of fabrication process of Na/C anode composites. Reproduced with permission.^[56] Copyright 2018, Wiley. c) Schematic of morphology change of Na foil and Na wood. Reproduced with permission.^[15] Copyright 2017, American Chemical Society. d) Schematic of the Na nucleation and deposition on a N,O codoped graphitized carbon-fiber electrode and a graphitized carbon-fiber electrode. Reproduced with permission.^[60] Copyright 2018, American Chemical Society. e) Schematic of the Na stripping/plating on Na foil and Na with a N,S codoped carbon nanotube paper as interlayer. Reproduced with permission.^[64] Copyright 2018, Wiley. f) Schematic of Na plating/stripping on BiCN@Cu foil. Reproduced with permission.^[83] Copyright 2021, Wiley.

and reduced local current density induced by the introduction of 3D Ni host.

Considering the high weight and cost of metals, carbon materials with a small weight and low cost are rather promising Na hosts.^[84,85] Chi et al.^[56] reported a 3D flexible commercial carbon felt as a sodium host. The Na/C composite was fabricated by immersing carbon felt into molten sodium by a facile molten-infusion strategy (Figure 4b). The carbon felt can prestore Na and accommodate further Na deposition, inducing a uniform Na⁺ flux, as well as alleviating the volume change. As a result, such Na/C composites showed a small overpotential of 35 mV after 120 cycles at a high current density of 5 mA cm⁻² with 2 mAh cm⁻² capacity in symmetric cells. Besides, carbonized wood with aligned channels was proposed as sodium host, and a Na wood composite was fabricated by molten-infusion method (Figure 4c).^[15] Owing to the merits of carbonized wood, such as channel structure offers, large surface area, and a highly conductive as well as mechanically stable skeleton, the local effective current density was reduced, a uniform Na nucleation and deposition was induced, and the volume change was restricted. As a result, the Na wood composite demonstrates a small overpotential and a stable cycling over 500 h at 1 mA cm⁻² with 1 mAh cm⁻² in symmetric cells. Similarly, an oxygen-containing carbon with a 3D tubular structure fabricated by carbonizing coconut framework was also developed as Na host and showed a promising electrochemical performance.^[57]

Furthermore, Wang et al.^[58] reported a Na@rGO composite making sodium metal anode processable and moldable. The Na@rGO composite was fabricated by adding graphite oxide

(GO) into molten sodium. Molten Na instantaneously reduced GO sheets to r-GO and was further absorbed into the r-GO sheets. The Na@rGO composite with 5 wt% of rGO retained 91% of the theoretical capacity of Na metal, showing an enhanced tensile strength and hardness as well as a low reactivity. Moreover, it could be easily molded into various shapes. The stable cycling of more than 600 h at 1.0 mA cm⁻² with 1.0 mAh cm⁻² was obtained in symmetric cells.

Carbon hosts doped with heteroatoms (such as N, S, O, etc.) are beneficial for improving wettability toward molten Na and guiding uniform Na nucleation due to the high adsorption energy toward Na. For example, a free-standing N-doped mesoporous carbon paper (CPPY) fabricated by carbonization of polypyrrole-coated nanocellulose paper was developed as a Na host.^[59] A larger surface area and N-doping of CPPY lowered the local current density and consequently Na-CPPY composites exhibited a small overpotential of 38 mV over 1000 h at a current density of 1 mA cm⁻² with 1 mAh cm⁻². Furthermore, N,O codoped graphitized carbon fibers (DGCF) also have been developed as Na hosts.^[60] DGCF were fabricated by refluxing GCF with H₂SO₄/HNO₃. Experimental results and first-principles calculations showed that nitrogen and oxygen served as sidiophilic sites to guide uniform Na nucleation due to the high binding energy toward Na (Figure 4d). As a result, excellent cycling stability over 1200 h at 2 mA cm⁻² with 1 mAh cm⁻² was obtained.

Other sidiophilic materials incorporated into the carbon host (such as Fe₂O₃,^[61] SnO₂,^[62] etc.) are also helpful for improving wettability of molten Na and inducing uniform Na nucleation. A Fe₂O₃-coated carbon cloth was developed as a Na host, and

molten sodium was successfully infiltrated into the structure.^[61] The highly conductive and mechanically robust Fe₂O₃-coated carbon cloth not only provided a stable scaffold but also reduced the current density and led to uniform nucleation and growth of sodium, resulting in a dendrite-free and highly stable Na metal anode. As a consequence, high cycling stability at 5 mA cm⁻² with 1 mAh cm⁻² over 300 cycles was obtained in symmetric cells. Similarly, SnO₂-coated carbon cloth was also fabricated as a Na host, and Na metal anode showed an improved cycling stability.^[62]

Another facile and straightforward method to stabilize the structure of Na metal is applying an interlayer, which would serve as a host after repeated Na stripping/plating. For example, Li et al.^[63] employed a commercial carbon paper as interlayer on the Na surface. The carbon paper layer with a large surface area improved the current distribution, inducing a uniform Na deposition. As a result, Na metal anodes with interlayer exhibited superior cycling stability at various current densities in both carbonate- and ether-based electrolytes. Besides, Sun et al.^[64] adopted a N,S co-doped carbon nanotube paper as an interlayer. The highly “sodiophilic” N- and S-containing groups on the carbon nanotubes surface can create a uniform Na nucleation and deposition, leading to a dendrite-free Na metal anode. As a result, excellent cycling stability was demonstrated in symmetric cells (Figure 4e). Furthermore, Sun et al.^[65] fabricated carbon nanotube (CNT) films with a sodiophobic–sodiophilic gradient across the thickness direction as interlayer by decorating sodiophilic Ag nanoparticles at the sodiophobic CNT walls to formulate an Ag-deficient layer at one side of the CNT film and an Ag-rich layer at the opposite side. Na preferentially plated at the Ag-rich layer near the current collector. The mechanically robust Ag-deficient CNT film layer near the separator acted toward blocking the Na dendrite formation. In addition, the highly conductive CNT film regulated the Na⁺ flux distribution. As a result, CNT film-based gradient interfacial layer enabled a stable cycling of 1000 h at a current density of 8 mA cm⁻².

Nucleation layers with sodiophilic materials (such as Bi,^[83] Sn,^[86] Sb,^[66] etc.) as a coating on the current collector can smoothen the Na deposition due to the formation of alloys with a low Na nucleation energy. For example, Zhang et al.^[83] fabricated bismuth-embedded carbon nanosheets (Bi/CNs) as a Na nucleation layer. The formation of sodiophilic Na₃Bi alloy enabled the uniform nucleation and deposition of Na due to a low nucleation barrier for Na (Figure 4f). As a result, the cell using the Bi/CNs@Cu current collector showed a stable cycling for 7700 h with an average Coulombic efficiency (CE) of 99.92% at a high areal capacity of 3 mAh cm⁻². More importantly, a long cycling over 4000 h at 1 mA cm⁻² was obtained in symmetric cells with Bi/CNs@Cu.

3.1.2. Electrolyte Optimization

The reaction between the electrolyte and Na metal forms an SEI on the Na anode surface. Commonly, the SEI is electronically insulating but shows high ionic conductivity, which enables the Na⁺ transport and prevents the further reaction between the electrolyte and Na metal. The compositions of electrolyte (salts, solvent, and additives) affect the components of SEI, which

determine the stability and reversibility of the Na metal. Iermakova et al.^[87] comparatively investigated the composition, morphology, and stability of SEI formed on Li and Na in carbonate-based electrolytes. They found out that Na metal showed a less stable SEI verified by resistivity change with time, and a morphology change after the cyclic voltammetry test. Furthermore, Dugas et al.^[35] found out that the reaction between Na and electrolyte solvents occurred during whole time of investigations (between 5 and 48 d), and the SEI is extremely unstable by detecting different gases and oligomers formation. Seh et al.^[67] reported that more stable and robust SEI films in SMBs could be formed with the usage of NaPF₆ in glymes (mono-, di-, and tetra-) instead of conventional carbonated-based electrolytes (NaPF₆ in ethylene carbonate [EC]/diethyl carbonate [DEC] and NaPF₆ in EC/dimethylene carbonate [DMC]) (Figure 5a). The stable SEI in ether-based electrolytes mainly consisted of sodium oxide and sodium fluoride, which is impermeable to electrolyte solvents, preventing the further reaction between the electrolyte and the Na metal as well as reducing the Na dendrite formation. As a result, a high average CE of 99.99% was obtained over 300 cycles at 0.5 mA cm⁻² in Cu|Na half cell (Figure 5b) with the electrolyte containing 1 M NaPF₆ in diglyme. In contrast, a mixed organic–inorganic SEI was obtained in carbonated-based electrolytes, which is more permeable to electrolyte solvents. Another strategy for the SEI design on the Na surface is the utilization of highly concentrated electrolytes. Due to the high ionic concentration and less free solvents, high concentration electrolytes can induce a compact SEI, prolong the Sand's time, prevent the corrosion of the current collector, and improve oxidation stability of the electrolyte at high voltages. For example, Zhang's group explored a highly concentrated sodium bis(fluorosulfonyl)imide (NaFSI) in glymes (4 mol L⁻¹). Such electrolyte not only endowed a highly reversible Na deposition and stripping with a high CE of 99% at 1.0 mA cm⁻² in half cell, but also enabled a long-term cycling stability in SMBs paired with a Na₃V₂(PO₄)₃ cathode. This excellent electrochemical performance was ascribed to the formation of compact inorganic SEI films and thus reduced side reactions.^[68] However, the high viscosity, poor wettability, and increased cost of highly concentrated electrolytes hindered their practical application. To overcome the disadvantage of the highly concentrated electrolytes, a localized high concentration electrolyte (2.1 M NaFSI/DME-bis(2,2,2-trifluoroethyl) ether (BTFE) (solvent molar ratio 1:2)) was prepared using hydrofluoroether as an “inert” diluent by Zheng et al.^[88] Because hydrofluoroether does not break the localized Na⁺-FSI⁻DME solvation structure but reduces the viscosity and increases the conductivity, excellent performance was demonstrated, outperforming that of 5.2 M NaFSI/DME.

Apart from altering the solvents and salts in the electrolyte, adopting additives is another effective method to form a stable SEI or control the Na deposition. For example, Wu et al.^[69] fabricated a NaF-rich protection film on Na by using fluoroethylene carbonate (FEC) additive (2 wt%) in the electrolyte. The NaF-rich protection film prevented side reactions and suppressed the Na dendrite formation. As a result, long-term stable cycling was achieved in symmetric cells in Ar gas and O₂ gas. More importantly, the assembled Na–O₂ batteries showed an improved cycling stability at a large current density of 500 mAh g⁻¹. Besides, Zheng et al.^[70] fabricated a Na–Sn alloy layer and

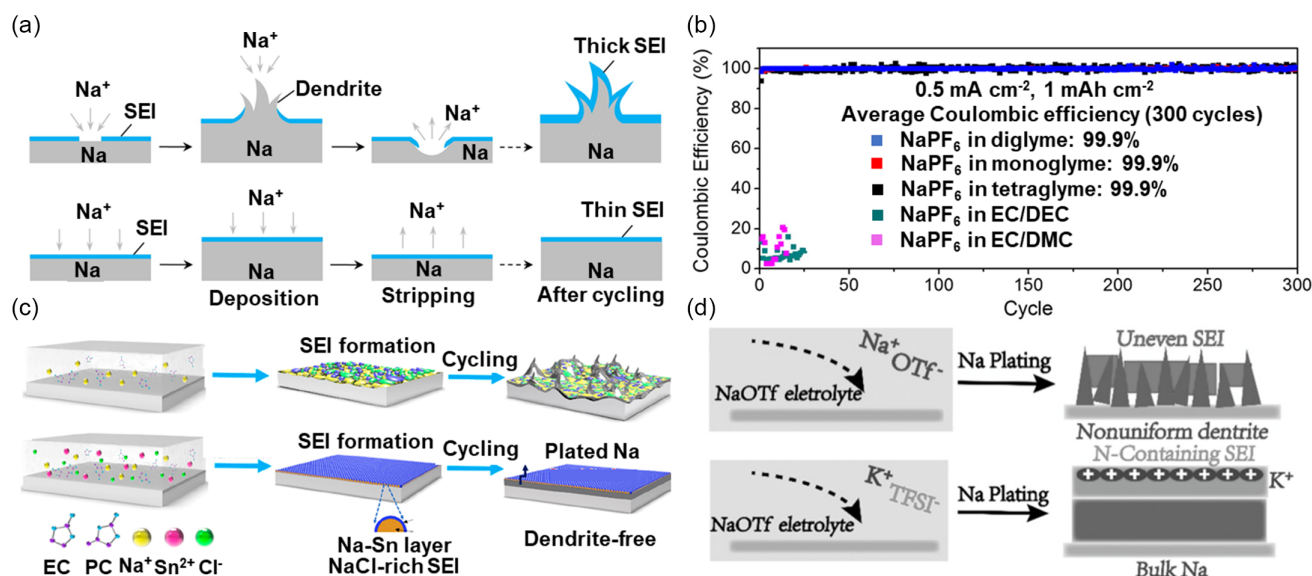


Figure 5. a) Schematics of Na morphology with different SEI after cycling. b) Coulombic efficiencies of Na metal using 1 M NaPF₆ in various electrolytes during plating/stripping process. Reproduced under the terms of ACS AuthorChoice/Editors' Choice license.^[67] Copyright 2015, The Authors. Published by American Chemical Society. c) Schematics of morphology of Na foil and Na foil with a Na-Sn alloy layer plus a NaCl-rich SEI after cycling. Reproduced with permission.^[70] Copyright 2019, American Chemical Society. d) Schematics of Na deposition from NaOTf electrolyte and from the NaOTf electrolyte with a potassium trifluoromethanesulfonimide (KTFSI) additive. Reproduced with permission.^[71] Copyright 2018, Wiley.

NaCl-rich SEI by adding SnCl₂ (50 mM) as additive into electrolyte. This designed SEI not only enabled a rapid interfacial ion transfer due to the alloy phase and NaCl, but also prevented side reactions between Na and the electrolyte due to the physical barrier effect (Figure 5c). Consequently, stable cycling over 500 h at 0.5 mA cm⁻² with 1 mAh cm⁻² was obtained in symmetric cells. Furthermore, cations can be used as additives to guide uniform Na deposition by electrostatic shielding.^[89] Cations with a lower reduction potential than Na⁺ can preferentially be adsorbed on the tip and form an electrostatic shield. The cation shield layer would push Na⁺ away from the tip and prevent the dendrite formation. For example, K⁺ was used as a cation additive for uniform Na deposition by using KTFSI as an additive.^[71] The K⁺ accumulated on protrusions of Na and formed electrostatic shield and prevented dendrite formation. In addition, TFSI⁻ decomposed into Li₃N and oxynitrides, which acted as SEI (Figure 5d). As a result, a stable cycling over 480 h at 2 mA cm⁻² with 10 mAh cm⁻² was obtained in symmetric cells.

3.1.3. Interface Engineering

Apart from modifying the electrolyte to get the desired stable SEI, fabricating artificial SEI by ex situ physical methods or in situ chemical methods is also an effective strategy. For example, Luo et al.^[72] reported Al₂O₃ layers deposited on the Na metal by a low-temperature plasma-enhanced atomic layer deposition (ALD) method. The Al₂O₃ acted as an artificial SEI to prevent side reactions between Na and the electrolyte (Figure 6a). Consequently, a stable cycling with a small overpotential for 450 h at 0.25 mA cm⁻² was achieved. Zhao et al.^[73] also fabricated an Al₂O₃ layer deposited on Na by the ALD method. The Al₂O₃ layer suppressed Na dendrite formation and thus

improved battery lifetime. As a consequence, the optimized Al₂O₃ layer enabled a stable performance over 500 cycles at a current density of 3 mA cm⁻² with 1 mAh cm⁻². Furthermore, an artificial SEI consisting of Na₂S was fabricated through a conversion reaction between MoS₂ and Na in the Na-MoS₂ mixture.^[74] In addition, the residual MoS₂ nanosheets in Na-MoS₂ mixture acted as a 3D host to accommodate the volume change. As a result, Na-MoS₂ showed a long cycle life of 1000 cycles with a low overpotential of 25 mV at 0.2 mA cm⁻². Besides, Wang et al.^[90] adopted an ultrathin graphene film as artificial SEI on Na metal. The graphene film acted as a physical barrier to prevent side reactions between Na and the electrolyte, and enabled ionic diffusion due to the presence of defects (Figure 6b). They also found out that the graphene film with a thickness of ≈2.3 nm is suitable for low current densities (≤1 mA cm⁻²), and the graphene film with a thickness of ≈5 nm is suitable for high current densities up to 2 mA cm⁻². As a result, a stable cycling over 100 cycles at 2 mA cm⁻² with 3 mAh cm⁻² capacity was obtained. Furthermore, Wei et al.^[75] developed ionic membranes on the Na metal by polymerization of ionic liquids. Such membranes prevented side reactions with electrolytes and enabled fast ion transport. Consequently, high CE and a stable cycling even at high current densities were obtained. Besides, Kim et al.^[76] prepared free-standing inorganic-organic protective layers consisting of Al₂O₃ and polyvinylidene fluoride (PVDF). Propylene carbonate was introduced to create the pores for accommodating the liquid electrolyte. The protective layer not only mechanically suppressed the Na dendrite formation due to the high shear modulus and ionic conductivity, but also reduced electrolyte decomposition (Figure 6c). As a result, Na metal with the optimized protective layer showed a prolonged cycling life. Although the strategy of fabricating an artificial

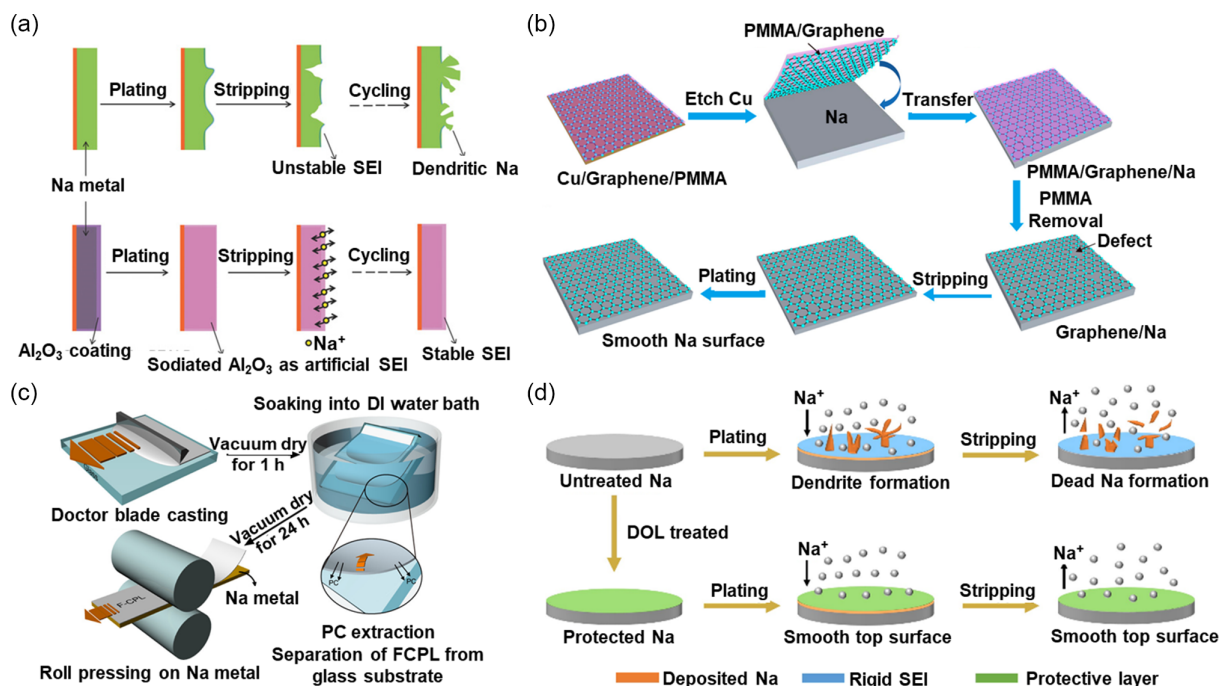


Figure 6. a) Schematic of morphology change of Na foil and Na foil with Al_2O_3 coating after cycling. Reproduced with permission.^[72] Copyright 2017, Wiley. b) Schematic of Na preparation with a graphene film as protective layer and the morphology after Na plating/stripping. Reproduced with permission.^[90] Copyright 2017, American Chemical Society. c) Schematic of the fabrication of a free-standing composite protective layer coated on Na metal (FCPL-Na). Reproduced with permission.^[76] Copyright 2017, American Chemical Society. d) Schematic of the Na plating and stripping behavior of untreated Na and protected Na. Reproduced under the terms of the CC BY 3.0 license.^[79] Copyright 2021, The Authors. Published by Royal Society of Chemistry.

SEI by physical ex situ processing showed improved electrochemical performance, the approach suffers from insufficient interfacial contacts.

Fabricating an artificial SEI by in situ chemical approach is a more promising strategy because of the improved interfacial contact. For example, Choudhury et al.^[77] fabricated a NaBr layer on Na metal by a bromopropane treatment. They experimentally confirmed the formation of NaBr, and found that NaBr is a low ion diffusion barrier. In situ visualization of Na deposition confirmed the improved stability of the Na anode. The NaBr layer on Na metal restricted dendrite formation and prevented side-reactions. Consequently, a stable cycling over 250 cycles with a low overpotential at 0.5 with 0.5 mA cm^{-2} capacity was obtained in symmetric cells. Besides, Ma et al.^[78] prepared bismuth layers on the Na metal anode by a $\text{Bi}(\text{SO}_3\text{CF}_3)_3$ -DME solution treatment. The Bi-layer with fast charge-transfer kinetics suppressed the dendrite formation, as a result demonstrated a prolonged cycling for 1000 h at 0.5 mA cm^{-2} . Furthermore, Lu et al.^[79] developed in situ polymerization of 1,3-dioxolane (DOL) on Na metal surface by pretreating Na in DOL (Figure 6d). The artificial SEI composed of poly(DOL) enabled a fast interfacial transport and a lower resistance, suppressed the dendrite formation and gas evolution. As a result, a long-term cycling over 2800 h at 1 mA cm^{-2} was achieved in symmetric cells, while improved electrochemical performance was obtained in full cells paired with different cathodes. Interestingly, they also presented a spray DOL process which showed a promising for large-scale manufacturing of stable Na.

3.2. Strategies for Sodium Metal Stabilization in SSBs

The development of SSBs is plagued by the high interfacial charge transfer resistance owing to unfavorable physical contact and poor interfacial stability between Na metal anode and SSEs increased by the volume changes of the Na metal during charge/discharge cycles and Na dendrites formation.^[38,91] In order to address the challenges of the sodium metal anode, solutions including structure stabilization, electrolyte optimization, improving contact by mechanical methods, and interface engineering via chemical methods have been developed. The summary of various methods for stabilizing Na metal anode in SSBs is listed in Table 2.

3.2.1. Structure Stabilization

In SSBs, an effective host for Na metal is essential to accommodate the volume change of Na for enabling the intimate interfacial contact between SSEs and Na metal because the rigid inorganic solid electrolyte cannot deform when volume changes happen during Na plating/stripping. Na alloys can serve as electron- and ion-conductive hosts because their framework can offer continuous pathways for electrons and Na^+ ions allowing Na stripping and plating, and maintaining a seamless interface contact with SSEs, leading to a dendrite-free morphology.^[106] In addition, the alloys are also capable to form a stable interface due to the reduced reactivity with the SSEs as compared

Table 2. Comparison of performance of solid-state sodium batteries (SSBs). SSE, solid-state electrolyte; CCD, critical current density.

Strategy	Performance	References
Na ₁₅ Sn ₄ alloy as anode and NZSP as SSE.	High CCD of 2.5 mA cm ⁻² ; over 500 cycles at 0.5 mA cm ⁻² in the symmetric cells.	[92]
Na–Sn alloy with acetylene black additive as anode and Na ₃ PS ₄ as SSE.	The full cells with SSE-coated Mo ₆ S ₈ cathodes can be cycled over 500 cycles at 60 mA g ⁻¹ within a voltage range of 0.9–1.9 V.	[93]
SnO ₂ -coated NZSP framework infused with Na metal as anode and NZSP as SSE.	Stable cycling for 700 h at 1 mA cm ⁻¹ with a capacity of 5 mAh cm ⁻² .	[94]
Annealing the NZSP to form a partially reduced surface.	A low interfacial resistance of 11 Ω cm ² and high CCD of 0.9 mA cm ⁻² .	[95]
Yttria-stabilized zirconia-enhanced Na-β"-Al ₂ O ₃ (YSZ@BASE) SSE.	Low interfacial resistance of 3.6 Ω cm ² and high CCD of 7.0 mA cm ⁻² at a capacity of 3.5 mAh cm ⁻² at 80 °C.	[96]
Introducing 10 wt% Na ₂ B ₄ O ₇ as sintering additive into Na ₃ Zr ₂ Si ₂ PO ₁₂ as SSE.	Interfacial resistance of 36 Ω cm ² , CCD of 0.55 mA cm ⁻² , over 2500 h cycles stability at 0.3 mA cm ⁻² with a capacity of 0.3 mAh cm ⁻² .	[97]
Introducing rare-earth oxides into NZSP during sintering to adjust the Si/P ratio at grain boundaries.	High CCD values were realized up to 0.85 and 0.65 mA cm ⁻² were realized with Sm ₂ O ₃ and Ho ₂ O ₃ , respectively.	[98]
Applying the stack pressure between Na metal and BASE.	–	[99]
By simple mechanical compression of Na/Na ₃ Zr ₂ Si ₂ PO ₁₂ .	Interfacial resistance of 14 Ω cm ² .	[100]
Alucone film deposited on Na ₃ PS ₄ and Na ₃ SbS ₄ prepared by molecular layer deposition.	Stable cycling over 475 h in the symmetric cells.	[101]
Graphene-deposited Na ₃ Zr ₂ Si ₂ PO ₁₂ with chemical vapor deposition.	Achieved a 10-fold reduction in interfacial resistance from 524 to 46 Ω cm ² ; stable cycling over 1000 h at 1 mA cm ⁻² with a capacity of 1 mAh cm ⁻² .	[102]
Fluorinated amorphous carbon coated Na ₃ Zr ₂ Si ₂ PO ₁₂ reacted with Na metal to produce in situ NaF layer.	A symmetric cell showed a stable cycling below 0.6 mA cm ⁻² .	[103]
By exposing Na ₃ SbS ₄ in ambient air for 10 min to in situ form an interlayer of NaH and Na ₂ O.	A low and stable polarization voltage can be realized.	[104]
The Cl-containing Na _{3-x} PS _{4-x} Cl _x can in situ react with Na metal to form NaCl interlayer.	CCD can reach up to 1.2 mA cm ⁻² .	[105]

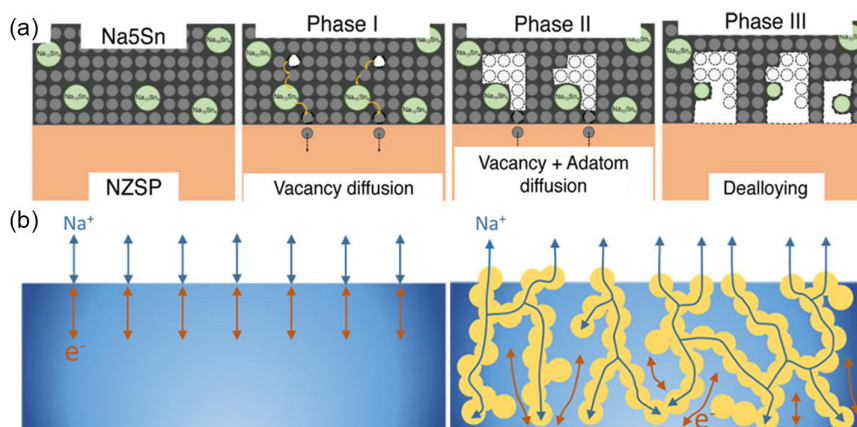


Figure 7. a) Na_xSn anodes are composed of two different Na sources (metallic Na and Na₁₅Sn₄) during the desodiation process. Three distinct phases were found in the Na_xSn–NZSP cells; I) both the ASR and interfacial capacitance remained constant at the initial stage, followed by II) a slow increasing in ASR but rapidly decreasing interfacial capacitance, and finally, III) a rapidly decreasing ASR but constant capacitance. These provide vital information on the diffusion mechanism during Na desodiation in Na_xSn–NZSP cells. Reproduced with permission.^[92] Copyright 2021, Wiley. b) Schematic illustrations of cycle-induced interface evolution in pristine Na/SSE interface (left) and hybrid Na/SSE interface (right). Reproduced with permission.^[94] Copyright 2021, Elsevier.

with Na metal. Oh et al.^[92] constructed a robust physical contact between the Na anode and the SSE NZSP (**Figure 7a**). The addition of Na₁₅Sn₄ in the Na matrix increases the Na⁺ diffusivity in the anode layer that reduces the tendency to form

pores at the interface, which shows a high CCD of 2.5 mA cm⁻² and a stable galvanostatic cycling for more than 500 cycles at 0.5 mA cm⁻² in the symmetric cells. The alloy strategy is not only adopted successfully in oxide-based SSEs, but sulfide-based SSEs

can also be used to ameliorate the interfacial contact between the Na metal and SSE by utilizing a Na–Sn alloy instead of Na metal as the anode. Yue et al.^[93] assembled an SSBs with a Na–Sn alloy with acetylene black additive as anode, Na₃PS₄ as SSE, and SSE-coated Mo₆S₈ as cathode, which also demonstrated an improved interfacial contact between the anode and SSE. Furthermore, Cao et al.^[94] designed a robust bulk-hybrid Na metal anode using a facile melt infusion process in which molten Na was mixed with surface-modified Na_{3.4}Zr₂Si_{2.4}P_{0.6}O₁₂ (NZSP). A conformal SnO₂ layer was precoated on the surface of the NZSP particles for better affinity with molten Na, in which SnO₂ can react with Na to form Na–Sn alloy during heating to significantly improve the wettability of Na (Figure 7b). A fast and continuous pathway for simultaneous transportation of electrons and Na⁺ is established throughout the composite anode. Benefiting from the intimate anode configuration, it delivered stable cycling for 700 h at the current density of 1 mA cm^{−2} with a capacity of 5 mAh cm^{−2}.

3.2.2. Electrolyte Optimization

The mechanical strength of the SSE is a vital important property that can be strongly correlated with the Na dendritic growth across the electrolyte during repetitive cycling.^[107] The elastic modulus (*E*), e.g., Young's modulus and shear modulus, of the electrolyte is considered to be partially related to the dendrite formation on the Na surface. Monroe et al.^[108] and Albertus et al.^[109] suggested that the shear modulus of SSE should be at least twice that of the metal, which is 3.3 GPa for the bulk Na metal. In practical terms, the dendritic growth could still occur even if the SSE satisfies this criterion due to other factors that can also induce dendrite formation, like voids at the Na|SSE

interface^[45] and high electronic conductivity in the grain boundaries.^[110] Hardness (*H*) of the SSE represents the resistance to elastic and plastic deformation, or failure under external force, which is another important mechanical property. The *H* value of the SSE indicates its ability to tolerate the volume change of the electrodes and thus affects the interfacial contact between Na metal and SSE. *H* is inversely correlated with the fracture toughness *K*_{IC} (Equation (13)), which reflects the susceptibility to fracture and penetration of Na dendrites^[111]

$$K_{IC} = k \left(\frac{E}{H} \right)^{\frac{1}{2}} \frac{P}{c^{\frac{3}{2}}} \quad (13)$$

where *k* is a constant depending on the tested sample geometry (0.016 for the Vickers probe geometry^[112]), *P* is the applied loading, and *c* is the crack length.

The interface between SSE and Na metal can also be improved by modification of the SSE. For example, Oh et al.^[95] introduced a simple and cost-effective annealing process for the NZSP preparation and its interface with Na metal was improved. A simple annealing at 1000 °C eliminates adsorbed surface functional groups (e.g., hydroxyl groups and carbonate contamination) and forms a partially reduced surface. The annealed electrolyte showed that Si formed bonds with the surface functional groups when exposed to the ambient condition and a small interfacial resistance of 11 Ω cm² and a high CCD of 0.9 mA cm^{−2} (Figure 8a). Recently, Deng et al.^[96] reported that an yttria-stabilized zirconia (YSZ)-enhanced β"-Al₂O₃ solid electrolyte (YSZ@BASE) has an extremely low interface impedance of 3.6 Ω cm² with the Na metal anode at 80 °C, and also exhibits an extremely high CCD of ≈7.0 mA cm^{−2} at a capacity of 3.5 mAh cm^{−2} compared with those of other Li- and Na-ion solid electrolytes reported so far, which is almost five times

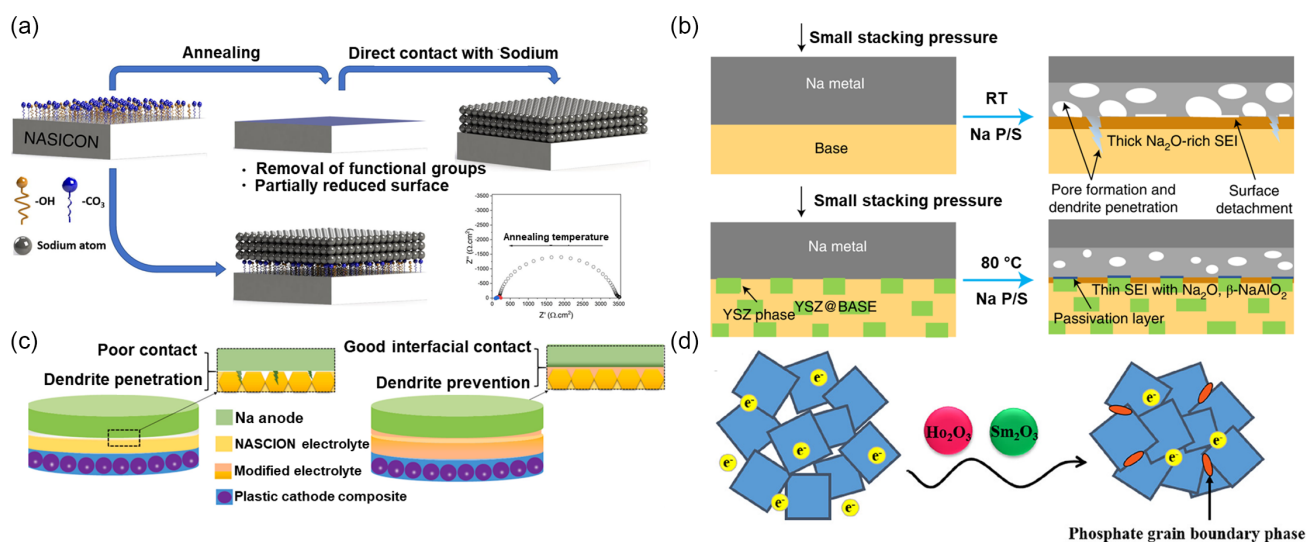


Figure 8. a) Schematic of annealing process during the NZSP preparation to improve its interface with Na metal. Reproduced with permission.^[95] Copyright 2021, Elsevier. b) Schematics of the Na plating/stripping mechanisms for BASE and YSZ@BASE to illustrate the interface anchoring effect and interphase formation. CE, counter electrode; WE, working electrode. Reproduced with permission.^[96] Copyright 2021, Springer Nature. c) Illustration of the grain-boundary-mediated ceramic electrolyte suppressing the Na dendrites in all-solid-state sodium batteries. Reproduced with permission.^[97] Copyright 2021, Elsevier. d) Schematic of the addition of rare-earth oxides in the sintering process. Reproduced with permission.^[98] Copyright 2022, American Chemical Society.

higher than that of pure BASE ($\approx 1.5 \text{ mA cm}^{-2}$) under similar testing conditions. YSZ plays a critical role in suppressing the Na dendrite penetration by enhancing the fracture toughness and lowering the overall electronic conduction of YSZ@BASE, which can prevent internal Na deposition (Figure 8b). As an oxygen-ion conductor, YSZ can also transport oxygen ions and thus eliminate oxygen vacancies caused by BASE reduction, which leads to formation of a thin and stable $\beta\text{-NaAlO}_2$ -rich interface, rather than a thicker Na_2O -rich interface for BASE.

For polycrystalline SSE materials, the ionic transport is controlled by the orientation of the grains and grain boundaries (sometimes also amorphous or secondary phases are involved). Therefore, the interface between SSE and Na metal can be improved by grain boundary design. For instance, Zhao et al.^[97] proposed a grain-boundary mediating strategy to stabilize the $\text{Na}|\text{Na}_3\text{Zr}_2\text{Si}_2\text{PO}_{12}$ interface and improve the capability of Na^+ ion transfer at the interface by introducing 10 wt% $\text{Na}_2\text{B}_4\text{O}_7$ as sintering additive (Figure 8c). The addition of $\text{Na}_2\text{B}_4\text{O}_7$ with a low melting point (741°C) into $\text{Na}_3\text{Zr}_2\text{Si}_2\text{PO}_{12}$ realized a highly dense microstructure and a lower sintering temperature from over 1200 to 1000°C . The interfacial resistance was reduced to $36 \Omega \text{ cm}^2$, with a higher CCD of 0.55 mA cm^{-2} and over 2500 h cycling stability at the current density of 0.3 mA cm^{-2} and capacity of 0.3 mAh cm^{-2} , resulting from the improved interfacial contact with Na metal and uniform stripping/plating upon the cycling. In addition, Wang et al.^[98] used the rare-earth oxides (Ho_2O_3 and Sm_2O_3) during the sintering process of NASICON, where the formed phosphate phase at grain boundaries adjusts the Si/P ratio in the NZSP structure with a higher Na^+ occupancy and hence promoting the ionic conductivity of electrolytes (Figure 8d). On the one hand, the formed phosphate phase with a low electronic conductivity prevents the transmission of electrons along the grain boundaries and reduces the probability that electrons combine with Na^+ at the grain boundary to form Na^0 , thereby restricting the formation and propagation of dendrites. On the other hand, the added rare-earth oxides act as flux agents, increasing the densification of NZSP, further enabling the enhancement of ionic conductivity and restricting dendrites in the voids. The obtained NZSP with 0.2 mol Sm_2O_3 and 0.3 mol Ho_2O_3 deliver CCD values of 0.85 and 0.65 mA cm^{-2} at room temperature, respectively.

3.2.3. Improving Contact by Mechanical Methods

Utilizing a ceramic electrolyte in SSBs has the potential to circumvent interfacial issues by mechanically constraining the plating of the Na metal by external pressure, improving even and dense deposition, therefore enabling stable $\text{Na}|\text{SSE}$ interfacial contact and high Coulombic efficiencies. Especially in the context of ASSBs, where the Na metal is compressed between a rigid metal current collector (Al, Cu, Ni plates, etc.) and SSE, the mechanical environment is totally different from conventional batteries using liquid electrolytes. As the geometry and morphology of a Na metal anode evolves upon charging/discharging (plating/stripping), the application of external pressure and deformation of Na metal play an important role in maintaining low interfacial resistances.

Recent reports have shown that applying an external pressure (stack pressure) can effectively improve the interface contact and suppress the formation of voids. Kasemchainan et al.^[41] suggested that a stacking pressure of 5–7 MPa can be favorable for Li metal stripping and plating during a steady electrochemical cycling. A 3D time-dependent model (Figure 9a) for tracking the evolution of interfaces formed between Na metal and $\text{Na}\beta\text{-Al}_2\text{O}_3$ was reported by Zhang et al.^[99] The differences due to contact elastoplasticity are larger than the differences in metal creep effects. The increased stack pressure can lead to lower creep due to a more conformal contact at the high pressure. Uchida et al.^[100] have successfully reduced the interfacial resistance as low as $14 \Omega \text{ cm}^2$ at room temperature by a simple mechanical compression of a $\text{Na}|\text{Na}_3\text{Zr}_2\text{Si}_2\text{PO}_{12}$ (NASICON) assembly (Figure 9b). Their work also demonstrated an advantage of the $\text{Na}|\text{NASICON}$ interface in comparison to the $\text{Na}\beta\text{-Al}_2\text{O}_3$ counterpart by means of the electrochemical impedance technique, which elucidated a significant difference between the activation energies for interfacial charge transfer: $\approx 0.6 \text{ eV}$ for $\text{Na}|\text{NASICON}$ and $\approx 0.3 \text{ eV}$ for $\text{Na}|\text{Na}\beta\text{-Al}_2\text{O}_3$. They suggested the formation of a Na^+ -conductive interphase layer by pressing Na metal on the NASICON surface.

3.2.4. Interface Engineering via Chemical Methods

To improve the stability of the interface between SSE and Na, different functional interlayers have been investigated. For

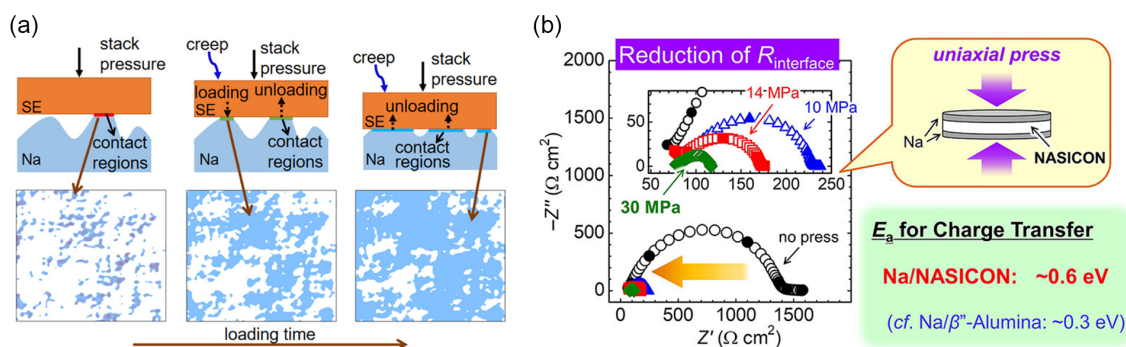


Figure 9. a) A 3D time-dependent model for tracking the evolution of interfaces formed between Na metal and $\text{Na}\beta\text{-Al}_2\text{O}_3$. Reproduced with permission.^[99] Copyright 2021, American Chemical Society. b) Schematic of the insights into Na^+ ion transfer at $\text{Na}|\text{NASICON}$ interface improved by uniaxial compression. Reproduced with permission.^[100] Copyright 2019, American Chemical Society.

example, an alucone film prepared by molecular layer deposition (MLD) has been employed to limit the decomposition of sulfide-based electrolytes (Na_3SbS_4 and Na_3PS_4) and suppress the Na dendrite growth (Figure 10a).^[101] Such a strategy effectively improves the room-temperature cycling stability for over 475 h in Na–Na symmetric cells due to the synergistic effect between the dendrite-suppressed sodiated alucone

(Na–Al–C–O) and the insulating unsodiated alucone (Al–C–O). Besides, Matios et al.^[102] employed the CVD system toward the direct growth of graphene-like interlayer on NASICON ceramic electrolyte, achieving a tenfold reduction in interfacial resistance (from 524 to 46 $\Omega\text{ cm}^2$) and over 1000 h of cycling stability at the current density of 1 mA cm^{-2} and capacity of 1 mAh cm^{-2} (Figure 10b). The abundantly distributed network

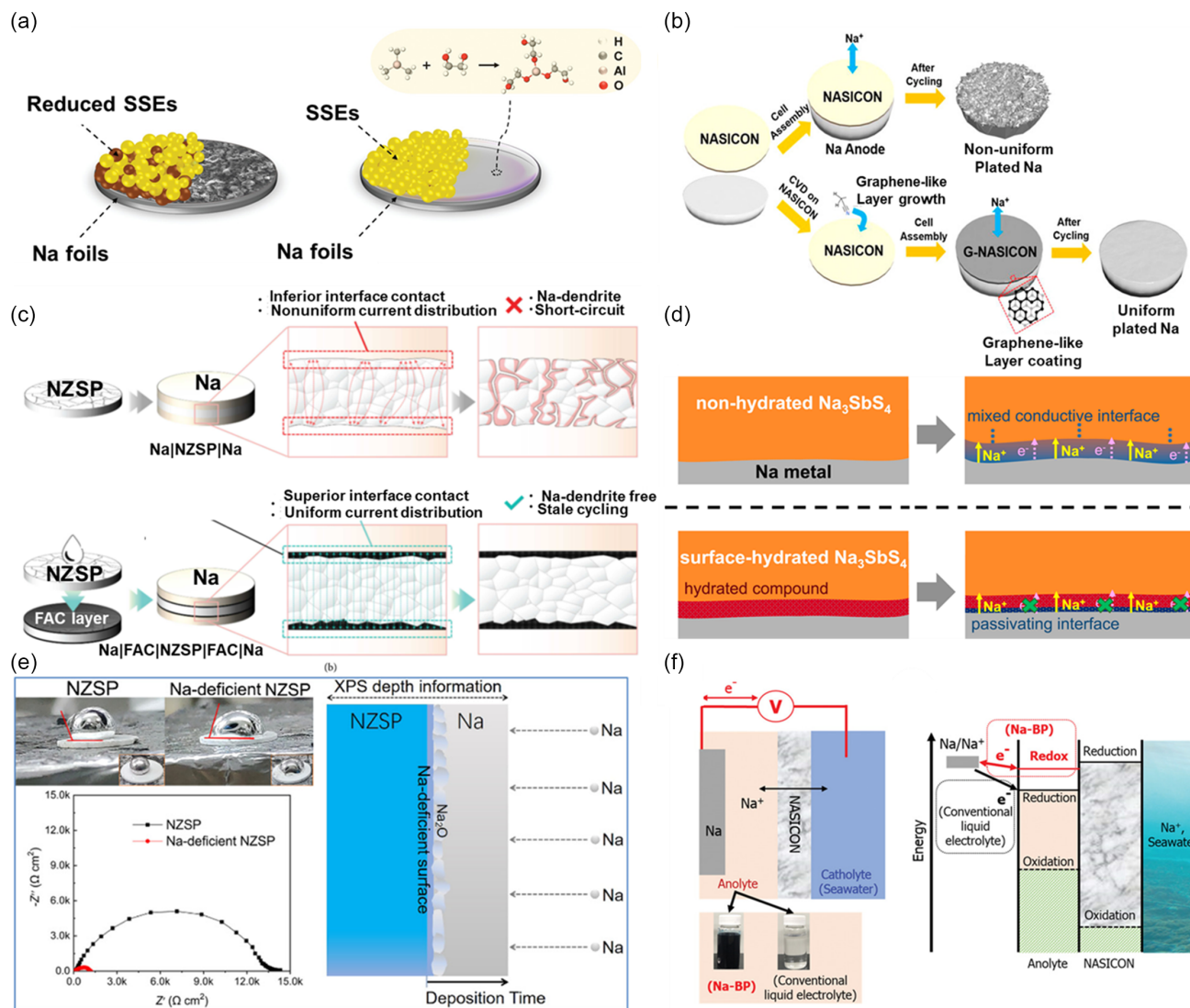
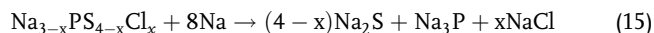
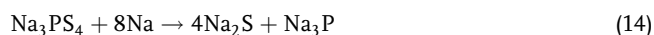


Figure 10. a) Schematic diagram of the reactive Na|sulfide-based SSEs interface and stable Na@alucone|sulfide-based SSEs interface. Reproduced with permission.^[101] Copyright 2020, Wiley. b) Schematic diagram of Na^+ ion plating/stripping using pristine and graphene-regulated NASICON (G-NASICON) electrolyte. For pristine NASICON electrolyte, a nonuniform and dendritic morphology formed after cycling. The chemical vapor deposition (CVD)-coated G-NASICON effectively suppressed the dendrite Na formation, resulting in a uniformly plated Na anode. Reproduced with permission.^[102] Copyright 2019, American Chemical Society. c) Schematic illustrations of the Na dendrite propagation in the unmodified NASICON pellet and suppression in the modified NASICON pellet. Reproduced under the terms of the CC BY 4.0 license.^[103] Copyright 2021, The Authors. Published by Beijing Institute of Technology Press. d) Schematic illustration of solid electrolyte|Na metal interface before (left) and after (right) electrochemical cycling. A mixed conductive interface layer grew during cycling of the nonhydrated Na_3SbS_4 (top), whereas a passivating interface was formed on the hydrated compound of the surface-hydrated Na_3SbS_4 (bottom). Reproduced under the terms of the CC BY-NC-ND 4.0 license.^[104] Copyright 2019, The Authors. Published by Elsevier. e) Contact angle measurement of molten metallic Na on NZSP SSE and Na-deficient NZSP. Comparison of EIS profiles of the symmetric cells of Na|NZSP|Na and Na|NZSP (HT)|Na. Schematic model of the proposed interface growth during the stepwise adsorption of metallic Na. Reproduced with permission.^[114] Copyright 2020, American Chemical Society. f) Illustrative overview of the general concept when employing Na-BP as anolyte in Na seawater batteries: The general cell setup with two photographs showing the Na-BP anolyte solution in comparison with a conventional liquid electrolyte (left). The energy diagram of the multilayer electrolyte system (right). Reproduced with permission.^[115] Copyright 2020, Wiley.

of defects on graphene-like interlayers can enable uniform Na^+ flux across the Na|SSE interface, preventing the preferential Na metal plating along the grain boundaries of NASICON and therefore suppressing dendrite growth. Furthermore, various in situ methods were developed for formation of desired interfaces. Zhang et al.^[103] developed a fluorinated amorphous carbon (FAC) layer coated on NASICON, which enables in situ formation of NaF when molten Na metal comes in contact with the FAC layer (Figure 10c). Na dendrites were effectively suppressed due to the NaF formation in the interface. To prevent the reaction between sulfide-based SSE and Na metal, an interlayer with high ionic conductivity and electronic resistivity composed of NaH and Na_2O was in situ formed by using the reaction between the Na and surface hydrated Na_3SbS_4 prepared by exposure of Na_3SbS_4 in ambient air for 10 min (Figure 10d).^[104] A significantly lower voltage increase occurred after cycling with the surface-hydrated Na_3SbS_4 as compared with its nonhydrated counterpart, indicating improved interfacial stability and effective protection provided by the hydrate layer, which effectively suppressed the electrolyte decomposition. Miao et al.^[113] introduced an interlayer of AlF_3 between Na anode and NASICON SSE and hence a Na^+ conducting buffer layer was formed in situ by a conversion reaction with Na during initial cycles, which showed a high CCD up to 1.2 mA cm^{-2} . Furthermore, ionically conducting and electronically insulating interlayer composed of NaCl was formed by using Cl-containing $\text{Na}_{3-x}\text{PS}_{4-x}\text{Cl}_x$ as SSE.^[105] It was found that for Na_3SbS_4 and Na_3PS_4 , the reaction-induced interlayer continuously grows into a thick layer, impeding electrochemical performance. In sharp contrast, the Cl-containing SSE resulted in cells with better capacity retention compared to undoped Na_3PS_4 . The exsolution of the chloride content can passivate or stabilize the interface which was attributed to the decomposition product NaCl formed interlayer. The decomposition reactions can be written as



With Equation (15), the $\text{Na}_{3-x}\text{PS}_{4-x}\text{Cl}_x$ can be synthetically designed to yield an interlayer with a tunable NaCl content.

Using molten Na in combination with SSE is a well-known way to improve the contact area, but the large surface energy differences between the liquid Na metal and the SSE surface causes repulsion of the Na metal to appear as a bead on the SSE surface with large contact angle. Thus, it is necessary to engineer the surface energy of the SSE surface or molten Na to achieve a good wetting. Modification of SSEs compositions can form an interface that has smaller surface energy differences with molten Na leading to better wetting on the surface. As an example, the chemical reaction between Na and NZSP at 380°C resulted in a partially reduced NZSP surface (H-NASICON) that shows a better wettability toward molten Na and acted as a physical barrier separating the Na metal and the grain boundaries. Consequently, the H-NASICON showed a good cycling stability for 550 h, while the cell with NZSP was short-circuited after 1 h.^[116] A Na-deficient surface fabricated by thermal treatment also shows a decreased wettability angle of $\theta = 72.5^\circ$ and hence better sodium wettability than stoichiometric NZSP ($\theta = 122.5^\circ$)

(Figure 10e).^[114] First-principle calculation suggests that the sodium-deficient surface has dangling oxygen bonds that are more reactive to Na metal and thus increase the adhesion. A heat treatment on finely polished $\text{Na}-\beta''\text{-Al}_2\text{O}_3$ SSEs in argon atmosphere was also proposed by Bay et al.,^[117] which eliminated the surface hydroxyl groups and carbon contamination, hence reduced the ASR from hundreds of $\Omega \text{ cm}^2$ to $8 \Omega \text{ cm}^2$ and increased the CCD from 0.3 to 12 mA cm^{-2} at room temperature.

Alloying of Na with other elements, such as Sn, has shown that a change in the atomic environment can tune the surface energy. A composite anode consisting of Na and $\text{Na}_{15}\text{Sn}_4$ verified an increase of the Na^0 diffusivity in the anode layer and reduction of pore formation at the interface.^[92] Furthermore, Yang et al.^[118] employed a SnO_x/Sn film between Na metal and NZSP to improve the wettability and contact, and hence promoted uniform current distribution and inhibited the growth of Na dendrites. Alternatively, SiO_2 was added into molten Na to improve the wettability between NZSP and molten Na. The cross section of the cell showed that the formed Na-Si alloy has an intimate contact with the NZSP surface whereas gaps can be observed at the Na|NZSP interface. Compared to a Na|NZSP cell, the Na- SiO_2 |NZSP cell with close physical contact at the NASICON interface showed a reduced interfacial resistance from $1658 \Omega \text{ cm}^2$ to $101 \Omega \text{ cm}^2$.^[119] Furthermore, liquid metal anodes at room temperature are also favored due to their good contact with SSEs. Liquid sodium biphenyl (Na-BP) complex solutions was employed as an anolyte in a sodium-based battery system to physically separate the Na metal anode and NASICON ($\text{Na}_3\text{Zr}_2\text{Si}_2\text{PO}_{12}$),^[115] which can provide simultaneously a suitable electronic and ionic conductivity,^[120] reduce overpotential, and maintain high homogeneity during the plating process at the Na-BP anolyte|Na interface (Figure 10f). Due to its high reversibility and low redox potential (vs Na^+/Na), Na-BP can act as redox “mediator/carrier,” suppressing the parasitic reactions between Na metal and SSE and contributing to the reversible Na^+ ion storage. More interestingly, a Na-K alloys enabled excellent contact with SSE and realized high CCD in SSE batteries due to its liquid merit at room temperature.^[121,122] The biphasic Na-K alloy system faces more complicated ion competition when the stripping and plating processes occurs on both sides, which has been studied by Li et al. and they proposed a limiting dendrite growth model.^[123]

4. Conclusion and Outlook

In summary, the fundamental challenges of Na metal anode in batteries with organic liquid electrolyte and SSEs and corresponding strategies toward eliminating these challenges are presented. The mechanisms of suppressing the Na dendrite formation are intensively discussed. The strategy of structure stabilization implies accommodating the volume change and reducing local current density by applying hosts with a large surface area. The strategy of electrolyte optimization can help to suppress the side reactions and stabilize the interface. The strategy of interface engineering enables to avoid a direct contact between Na and the electrolyte and thus reduces the side reactions by introducing a coating layer. However, these strategies also

Table 3. Advantages and disadvantages of various methods for stabilization of sodium metal anode, for batteries with organic liquid electrolytes and solid-state electrolytes.

Strategy	Method	Advantage	Disadvantage
Structure stabilization	Electrochemical plating in the host structure	Capacity controllable	Inhomogeneous deposition
	Thermal molten infusion in the host structure	Common used	Complex fabrication process, inert atmosphere and thermal source required
	Mechanical rolling into the host	Simple and scalable fabrication process	High mechanical stability of host required
	Nucleation layer on current collector	Uniform deposition	Ineffective for high capacity Na plating
	Na alloy anode	Improved interfacial contact and reduced resistance	Reduced energy density for full cells
Electrolyte optimization	Composition modification	Composition designable	Probably reduced ionic transport and unknown SEI properties
	Additive	Simple and scalable	Continuous reaction until additive is exhausted
	High concentration organic liquid electrolyte	Stabilized SEI	High cost and high viscosity
	Local high concentration organic liquid electrolyte	Stabilized SEI	Relatively high cost
Interface engineering	Atomic layer deposition	Uniform deposition	Very complex fabrication process
	Solvent casting method	Low-cost and widely used technique	Inadequate interfacial contacts and uneven coating
	Wet chemical method	Simple and scalable	Uncontrollable reaction process
	Chemical vapor deposition	Uniform deposition and tunable coating composition	High substrate temperature required, a complex and expensive method
	Applying mechanical pressure	Simple and effective	Pressure equipment is required

possess some disadvantages. The large surface area of the applied host can induce more side reactions between the deposited Na and organic liquid electrolytes. The introduced coating layer normally increases the internal resistance and decelerates the ionic transport. In addition, advantages and disadvantages of various methodologies are listed in **Table 3**.

Although strategies dealing with structure stabilization, electrolyte optimization, and interface engineering have shown improved results with regard to a suppressing dendrite formation, there are still several challenges remaining to be addressed for the future development of SMBs. 1) Large amount of flammable gas is generated due to the reaction between the organic liquid electrolyte and highly reactive Na metal, which causes safety issue. The native surface film is always formed on the Na metal before usage; its impact on electronic and ionic conductivity should be studied; 2) Normally, unstable SEI is formed on Na metal surface in carbonate-based electrolyte. Although ether-based electrolytes are beneficial for stable SEI, it is challenging to combine it with a high voltage cathode for practical application due to their narrow stable voltage range. The interface is also formed when Na contacts a solid-state electrolyte. The fundamental study of SEI/interface regarding composition, crystalline, spatial structure, morphology nature, and their relationship to the ionic conductivity is interesting to conduct; 3). To fasten the development of Na metal for practical application, the electrochemical performance of Na metal anode should be tested under extreme conditions in pouch cell, such as lean organic liquid electrolyte/less solid-state electrolyte, low negative/positive capacity ratio, and high degree of discharge. Furthermore, advanced techniques for reducing the thickness of solid-state electrolyte should be developed, such as the tape casting

process.^[124] The failure of SMBs is induced by both factors, electrolyte depletion and dendrite growth with a following formation of inactive Na. In pouch cells with a limited electrolyte amount, the problem of depletion of electrolyte would be more serious. In addition, the lack of stack pressure in a pouch cell is another major challenge; and 4) Advanced in situ characterization is essential for monitoring Na metal anode during cycling, e.g., using in situ computed tomography with a 3D reconstruction to investigate the morphology change of Na metal, and applying in situ spectroscopy to monitor the chemical component change of the SEI or interphase are desirable. In addition, theoretical simulations are also beneficial to understand the working mechanisms of such strategies.

Acknowledgements

Q.L. and A.Y. contributed equally to this work. Q.L. and A.Y. acknowledge the financial support from China Scholarship Council (CSC, grant nos. 201808080137 and 201906200023). Financial support by the German Research Foundation (DFG) under the joint German-Russian DFG project “KIBSS” (grant no. 448719339) and the Federal Ministry of Education and Research (BMBF) under the project “HeNa” (grant nos. 03XP0390B and 03XP0390C) are acknowledged. A.O. likes to acknowledge the financial support from the Federal Ministry of Education and Research (BMBF) under the project “KaSiLi” (03XP0254D) in the competence cluster “ExcellBattMat.” The authors take responsibility for the content of this publication.

Open Access funding enabled and organized by Projekt DEAL.

Conflict of Interest

The authors declare no conflict of interest.

Keywords

electrolyte modification, interface engineering, sodium metal anodes, structure stabilization

Received: February 14, 2022

Revised: April 5, 2022

Published online: May 12, 2022

- [1] Z. Yang, J. Zhang, M. C. W. Kintner-Meyer, X. Lu, D. Choi, J. P. Lemmon, J. Liu, *Chem. Rev.* **2011**, 111, 3577.
- [2] J. B. Goodenough, K.-S. Park, *J. Am. Chem. Soc.* **2013**, 135, 1167.
- [3] C. Vaalma, D. Buchholz, M. Weil, S. Passerini, *Nat. Rev. Mater.* **2018**, 3, 18013.
- [4] X. Xiang, K. Zhang, J. Chen, *Adv. Mater.* **2015**, 27, 5343.
- [5] G. Fang, J. Zhou, A. Pan, S. Liang, *ACS Energy Lett.* **2018**, 3, 2480.
- [6] C. Delmas, *Adv. Energy Mater.* **2018**, 8, 1703137.
- [7] N. Yabuuchi, K. Kubota, M. Dahbi, S. Komaba, *Chem. Rev.* **2014**, 114, 11636.
- [8] B. Sun, Q. Lu, K. Chen, W. Zheng, Z. Liao, N. Lopatik, D. Li, M. Hantusch, S. Zhou, H. I. Wang, Z. Sofer, E. Brunner, E. Zschech, M. Bonn, R. Dronskowski, D. Mikhailova, Q. Liu, D. Zhang, M. Yu, X. Feng, *Adv. Mater.* **2022**, 34, 2108682.
- [9] Y. Liu, J. Li, Q. Shen, J. Zhang, P. He, X. Qu, Y. Liu, *eScience* **2022**, 2, 10.
- [10] Y.-F. Zhu, Y. Xiao, S.-X. Dou, Y.-M. Kang, S.-L. Chou, *eScience* **2021**, 1, 13.
- [11] H. Hou, X. Qiu, W. Wei, Y. Zhang, X. Ji, *Adv. Energy Mater.* **2017**, 7, 1602898.
- [12] M. Lao, Y. Zhang, W. Luo, Q. Yan, W. Sun, S. X. Dou, *Adv. Mater.* **2017**, 29, 1700622.
- [13] L. Li, Y. Zheng, S. Zhang, J. Yang, Z. Shao, Z. Guo, *Energy Environ. Sci.* **2018**, 11, 2310.
- [14] E. Matios, H. Wang, C. Wang, W. Li, *Ind. Eng. Chem. Res.* **2019**, 58, 9758.
- [15] W. Luo, Y. Zhang, S. Xu, J. Dai, E. Hitz, Y. Li, C. Yang, C. Chen, B. Liu, L. Hu, *Nano Lett.* **2017**, 17, 3792.
- [16] S. Wang, Y. Liu, K. Lu, W. Cai, Y. Jie, F. Huang, X. Li, R. Cao, S. Jiao, *Energy Fuels* **2021**, 35, 4587.
- [17] J. Lee, J. Kim, S. Kim, C. Jo, J. Lee, *Mater. Adv.* **2020**, 1, 3143.
- [18] H. Che, S. Chen, Y. Xie, H. Wang, K. Amine, X.-Z. Liao, Z.-F. Ma, *Energy Environ. Sci.* **2017**, 10, 1075.
- [19] E. Peled, D. Golodnitsky, G. Ardel, *J. Electrochem. Soc.* **1997**, 144, L208.
- [20] C. Bao, B. Wang, P. Liu, H. Wu, Y. Zhou, D. Wang, H. Liu, S. Dou, *Adv. Funct. Mater.* **2020**, 30, 2004891.
- [21] S. Wang, Y. Jie, Z. Sun, W. Cai, Y. Chen, F. Huang, Y. Liu, X. Li, R. Du, R. Cao, G. Zhang, S. Jiao, *ACS Appl. Energy Mater.* **2020**, 3, 8688.
- [22] Y. Zhao, K. R. Adair, X. Sun, *Energy Environ. Sci.* **2018**, 11, 2673.
- [23] X. Zheng, C. Bommier, W. Luo, L. Jiang, Y. Hao, Y. Huang, *Energy Storage Mater.* **2019**, 16, 6.
- [24] A. Pei, G. Zheng, F. Shi, Y. Li, Y. Cui, *Nano Lett.* **2017**, 17, 1132.
- [25] J. N. Chazalviel, *Phys. Rev. A* **1990**, 42, 7355.
- [26] Y. S. Cohen, Y. Cohen, D. Aurbach, *J. Phys. Chem. B* **2000**, 104, 12282.
- [27] J.-i. Yamaki, S.-i. Tobishima, K. Hayashi, S. Keiichi, Y. Nemoto, M. Arakawa, *J. Power Sources* **1998**, 74, 219.
- [28] C. Monroe, J. Newman, *J. Electrochem. Soc.* **2003**, 150, A1377.
- [29] C. Brissot, M. Rosso, J. N. Chazalviel, S. Lascaud, *J. Power Sources* **1999**, 81–82, 925.
- [30] D. Kashchiev, *J. Chem. Phys.* **1982**, 76, 5098.
- [31] H. Wang, E. Matios, J. Luo, W. Li, *Chem. Soc. Rev.* **2020**, 49, 3783.
- [32] D. R. Ely, R. E. García, *J. Electrochem. Soc.* **2013**, 160, A662.
- [33] A. Milchev, M. Irene Montenegro, *J. Electroanal. Chem.* **1992**, 333, 93.
- [34] W. Liu, P. Liu, D. Mitlin, *Chem. Soc. Rev.* **2020**, 49, 7284.
- [35] R. Dugas, A. Ponrouch, G. Gachot, R. David, M. R. Palacin, J. M. Tarascon, *J. Electrochem. Soc.* **2016**, 163, A2333.
- [36] X. Chen, X. Shen, B. Li, H.-J. Peng, X.-B. Cheng, B.-Q. Li, X.-Q. Zhang, J.-Q. Huang, Q. Zhang, *Angew. Chem., Int. Ed.* **2018**, 57, 734.
- [37] M. Goktas, C. Bolli, J. Buchheim, E. J. Berg, P. Novák, F. Bonilla, T. Rojo, S. Komaba, K. Kubota, P. Adelhelm, *ACS Appl. Mater. Interfaces* **2019**, 11, 32844.
- [38] J.A. S. Oh, L. He, B. Chua, K. Zeng, L. Lu, *Energy Storage Mater.* **2021**, 34, 28.
- [39] Y. Li, Z. Deng, J. Peng, E. Chen, Y. Yu, X. Li, J. Luo, Y. Huang, J. Zhu, C. Fang, Q. Li, J. Han, Y. Huang, *Chem. Eur. J.* **2018**, 24, 1057.
- [40] S. Wenzel, T. Leichtweiss, D. A. Weber, J. Sann, W. G. Zeier, J. Janek, *ACS Appl. Mater. Interfaces* **2016**, 8, 28216.
- [41] J. Kasemchainan, S. Zekoll, D. Spencer Jolly, Z. Ning, G. O. Hartley, J. Marrow, P. G. Bruce, *Nat. Mater.* **2019**, 18, 1105.
- [42] T. Krauskopf, H. Hartmann, W. G. Zeier, J. Janek, *ACS Appl. Mater. Interfaces* **2019**, 11, 14463.
- [43] M. Wang, J. B. Wolfenstine, J. Sakamoto, *Electrochim. Acta* **2019**, 296, 842.
- [44] D. Spencer Jolly, Z. Ning, J. E. Darnbrough, J. Kasemchainan, G. O. Hartley, P. Adamson, D. E. J. Armstrong, J. Marrow, P. G. Bruce, *ACS Appl. Mater. Interfaces* **2020**, 12, 678.
- [45] C.-L. Tsai, T. Lan, C. Dellen, Y. Ling, Q. Ma, D. Fattakhova-Rohlfing, O. Guillon, F. Tietz, *J. Power Sources* **2020**, 476, 228666.
- [46] K. Cao, X. Zhao, J. Chen, B. B. Xu, M. W. Shahzad, W. Sun, H. Pan, M. Yan, Y. Jiang, *Adv. Energy Mater.* **2021**, 2102579.
- [47] F. Sun, L. Duchêne, M. Osenberg, S. Risse, C. Yang, L. Chen, N. Chen, Y. Huang, A. Hilger, K. Dong, T. Arlt, C. Battaglia, A. Remhof, I. Manke, R. Chen, *Nano Energy* **2021**, 82, 105762.
- [48] W. Zhang, C.-D. Zhao, X.-L. Wu, *Adv. Mater. Interfaces* **2020**, 7, 2001444.
- [49] Y.-S. Hong, N. Li, H. Chen, P. Wang, W.-L. Song, D. Fang, *Energy Storage Mater.* **2018**, 11, 118.
- [50] R. Mogensen, D. Brandell, R. Younesi, *ACS Energy Lett.* **2016**, 1, 1173.
- [51] K. Miyazaki, N. Takenaka, E. Watanabe, Y. Yamada, Y. Tateyama, A. Yamada, *ACS Appl. Mater. Interfaces* **2020**, 12, 42734.
- [52] Y. Deng, J. Zheng, A. Warren, J. Yin, S. Choudhury, P. Biswal, D. Zhang, L. A. Archer, *Adv. Energy Mater.* **2019**, 9, 1901651.
- [53] T.-S. Wang, Y. Liu, Y.-X. Lu, Y.-S. Hu, L.-Z. Fan, *Energy Storage Mater.* **2018**, 15, 274.
- [54] S. Liu, S. Tang, X. Zhang, A. Wang, Q.-H. Yang, J. Luo, *Nano Lett.* **2017**, 17, 5862.
- [55] Q. Lu, X. Wang, A. Omar, D. Mikhailova, *Mater. Lett.* **2020**, 275, 128206.
- [56] S.-S. Chi, X.-G. Qi, Y.-S. Hu, L.-Z. Fan, *Adv. Energy Mater.* **2018**, 8, 1702764.
- [57] T. Li, J. Sun, S. Gao, B. Xiao, J. Cheng, Y. Zhou, X. Sun, F. Jiang, Z. Yan, S. Xiong, *Adv. Energy Mater.* **2021**, 11, 2003699.
- [58] A. Wang, X. Hu, H. Tang, C. Zhang, S. Liu, Y.-W. Yang, Q.-H. Yang, J. Luo, *Angew. Chem., Int. Ed.* **2017**, 56, 11921.
- [59] Z. Wang, M. Li, C. Ruan, C. Liu, C. Zhang, C. Xu, K. Edström, M. Strømme, L. Nyholm, *J. Phys. Chem. C* **2018**, 122, 23352.
- [60] Z. Zheng, X. Zeng, H. Ye, F. Cao, Z. Wang, *ACS Appl. Mater. Interfaces* **2018**, 10, 30417.
- [61] W.-S. Xiong, Y. Jia, Y. Xia, Y. Qi, W. Sun, D. He, Y. Liu, X.-Z. Zhao, *Chem. Commun.* **2018**, 54, 9406.
- [62] W.-S. Xiong, Y. Xia, Y. Jia, Y. Qi, W. Sun, D. He, Y. Liu, X.-Z. Zhao, *ACS Appl. Mater. Interfaces* **2018**, 10, 21254.
- [63] P. Li, T. Xu, P. Ding, J. Deng, C. Zha, Y. Wu, Y. Wang, Y. Li, *Energy Storage Mater.* **2018**, 15, 8.

- [64] B. Sun, P. Li, J. Zhang, D. Wang, P. Munroe, C. Wang, P. H. L. Notten, G. Wang, *Adv. Mater.* **2018**, *30*, 1801334.
- [65] Z. Sun, H. Jin, Y. Ye, H. Xie, W. Jia, S. Jin, H. Ji, *ACS Appl. Energy Mater.* **2021**, *4*, 2724.
- [66] G. Wang, Y. Zhang, B. Guo, L. Tang, G. Xu, Y. Zhang, M. Wu, H.-K. Liu, S.-X. Dou, C. Wu, *Nano Lett.* **2020**, *20*, 4464.
- [67] Z. W. Seh, J. Sun, Y. Sun, Y. Cui, *ACS Cent. Sci.* **2015**, *1*, 449.
- [68] R. Cao, K. Mishra, X. Li, J. Qian, M. H. Engelhard, M. E. Bowden, K. S. Han, K. T. Mueller, W. A. Henderson, J.-G. Zhang, *Nano Energy* **2016**, *30*, 825.
- [69] S. Wu, Y. Qiao, K. Jiang, Y. He, S. Guo, H. Zhou, *Adv. Funct. Mater.* **2018**, *28*, 1706374.
- [70] X. Zheng, H. Fu, C. Hu, H. Xu, Y. Huang, J. Wen, H. Sun, W. Luo, Y. Huang, *J. Phys. Chem. Lett.* **2019**, *10*, 707.
- [71] Q. Shi, Y. Zhong, M. Wu, H. Wang, H. Wang, *Angew. Chem., Int. Ed.* **2018**, *57*, 9069.
- [72] W. Luo, C.-F. Lin, O. Zhao, M. Noked, Y. Zhang, G. W. Rubloff, L. Hu, *Adv. Energy Mater.* **2017**, *7*, 1601526.
- [73] Y. Zhao, L. V. Goncharova, A. Lushington, Q. Sun, H. Yadegari, B. Wang, W. Xiao, R. Li, X. Sun, *Adv. Mater.* **2017**, *29*, 1606663.
- [74] D. Zhang, B. Li, S. Wang, S. Yang, *ACS Appl. Mater. Interfaces* **2017**, *9*, 40265.
- [75] S. Wei, S. Choudhury, J. Xu, P. Nath, Z. Tu, L. A. Archer, *Adv. Mater.* **2017**, *29*, 1605512.
- [76] Y.-J. Kim, H. Lee, H. Noh, J. Lee, S. Kim, M.-H. Ryou, Y. M. Lee, H.-T. Kim, *ACS Appl. Mater. Interfaces* **2017**, *9*, 6000.
- [77] S. Choudhury, S. Wei, Y. Ozhobes, D. Gunceler, M. J. Zachman, Z. Tu, J. H. Shin, P. Nath, A. Agrawal, L. F. Kourkoutis, T. A. Arias, L. A. Archer, *Nat. Commun.* **2017**, *8*, 898.
- [78] M. Ma, Y. Lu, Z. Yan, J. Chen, *Batteries Supercaps* **2019**, *2*, 663.
- [79] Q. Lu, A. Omar, L. Ding, S. Oswald, M. Hantusch, L. Giebeler, K. Nielsch, D. Mikhailova, *J. Mater. Chem. A* **2021**, *9*, 9038.
- [80] O. Guillon, J. Gonzalez-Julian, B. Dargatz, T. Kessel, G. Schierner, J. Räthel, M. Herrmann, *Adv. Eng. Mater.* **2014**, *16*, 830.
- [81] X. He, S. Jin, L. Miao, Y. Cai, Y. Hou, H. Li, K. Zhang, Z. Yan, J. Chen, *Angew. Chem., Int. Ed.* **2020**, *59*, 16705.
- [82] C. Chu, R. Li, F. Cai, Z. Bai, Y. Wang, X. Xu, N. Wang, J. Yang, S. Dou, *Energy Environ. Sci.* **2021**, *14*, 4318.
- [83] L. Zhang, X. Zhu, G. Wang, G. Xu, M. Wu, H.-K. Liu, S.-X. Dou, C. Wu, *Small* **2021**, *17*, 2007578.
- [84] Z. Li, K. Zhu, P. Liu, L. Jiao, *Adv. Energy Mater.* **2022**, *12*, 2100359.
- [85] Q. Lu, Y. Jie, X. Meng, A. Omar, D. Mikhailova, R. Cao, S. Jiao, Y. Lu, Y. Xu, *Carbon Energy* **2021**, *3*, 957.
- [86] G. Wang, F. Yu, Y. Zhang, Y. Zhang, M. Zhu, G. Xu, M. Wu, H.-K. Liu, S.-X. Dou, C. Wu, *Nano Energy* **2021**, *79*, 105457.
- [87] D. I. Iermakova, R. Dugas, M. R. Palacín, A. Ponrouch, *J. Electrochem. Soc.* **2015**, *162*, A7060.
- [88] J. Zheng, S. Chen, W. Zhao, J. Song, M. H. Engelhard, J.-G. Zhang, *ACS Energy Lett.* **2018**, *3*, 315.
- [89] F. Ding, W. Xu, G. L. Graff, J. Zhang, M. L. Sushko, X. Chen, Y. Shao, M. H. Engelhard, Z. Nie, J. Xiao, X. Liu, P. V. Sushko, J. Liu, J.-G. Zhang, *J. Am. Chem. Soc.* **2013**, *135*, 4450.
- [90] H. Wang, C. Wang, E. Matios, W. Li, *Nano Lett.* **2017**, *17*, 6808.
- [91] B. Tang, Y. Zhao, Z. Wang, S. Chen, Y. Wu, Y. Tseng, L. Li, Y. Guo, Z. Zhou, S.-H. Bo, *eScience* **2021**, *1*, 194.
- [92] J. A. S. Oh, J. Sun, M. Goh, B. Chua, K. Zeng, L. Lu, *Adv. Energy Mater.* **2021**, *11*, 2101228.
- [93] J. Yue, X. Zhu, F. Han, X. Fan, L. Wang, J. Yang, C. Wang, *ACS Appl. Mater. Interfaces* **2018**, *10*, 39645.
- [94] K. Cao, Q. Ma, F. Tietz, B. B. Xu, M. Yan, Y. Jiang, *Sci. Bull.* **2021**, *66*, 179.
- [95] J. A. S. Oh, Y. Wang, Q. Zeng, J. Sun, Q. Sun, M. Goh, B. Chua, K. Zeng, L. Lu, *J. Colloid Interface Sci.* **2021**, *601*, 418.
- [96] T. Deng, X. Ji, L. Zou, O. Chiekezi, L. Cao, X. Fan, T. R. Adebisi, H.-J. Chang, H. Wang, B. Li, X. Li, C. Wang, D. Reed, J.-G. Zhang, V. L. Sprenkle, C. Wang, X. Lu, *Nat. Nanotechnol.* **2022**, *17*, 269.
- [97] Y. Zhao, C. Wang, Y. Dai, H. Jin, *Nano Energy* **2021**, *88*, 106293.
- [98] X. Wang, W. Mei, J. Chen, D. Wang, Z. Mao, *ACS Appl. Energy Mater.* **2022**, *5*, 777.
- [99] X. Zhang, Q. J. Wang, B. Peng, Y. Wu, *ACS Appl. Mater. Interfaces* **2021**, *13*, 26533.
- [100] Y. Uchida, G. Hasegawa, K. Shima, M. Inada, N. Enomoto, H. Akamatsu, K. Hayashi, *ACS Appl. Energy Mater.* **2019**, *2*, 2913.
- [101] S. Zhang, Y. Zhao, F. Zhao, L. Zhang, C. Wang, X. Li, J. Liang, W. Li, Q. Sun, C. Yu, J. Luo, K. Doyle-Davis, R. Li, T. K. Sham, X. Sun, *Adv. Funct. Mater.* **2020**, *30*, 2001118.
- [102] E. Matios, H. Wang, C. Wang, X. Hu, X. Lu, J. Luo, W. Li, *ACS Appl. Mater. Interfaces* **2019**, *11*, 5064.
- [103] Q. Zhang, Y. Lu, W. Guo, Y. Shao, L. Liu, J. Lu, X. Rong, X. Han, H. Li, L. Chen, Y.-S. Hu, *Energy Mater. Adv.* **2021**, *2021*, 1.
- [104] Y. Tian, Y. Sun, D. C. Hannah, Y. Xiao, H. Liu, K. W. Chapman, S.-H. Bo, G. Ceder, *Joule* **2019**, *3*, 1037.
- [105] E. A. Wu, C. S. Kompella, Z. Zhu, J. Z. Lee, S. C. Lee, I. H. Chu, H. Nguyen, S. P. Ong, A. Banerjee, Y. S. Meng, *ACS Appl. Mater. Interfaces* **2018**, *10*, 10076.
- [106] S. Ye, L. Wang, F. Liu, P. Shi, Y. Yu, *eScience* **2021**, *1*, 75.
- [107] B. Tang, P. W. Jaschin, X. Li, S.-H. Bo, Z. Zhou, *Mater. Today* **2020**, *41*, 200.
- [108] C. Monroe, J. Newman, *J. Electrochem. Soc.* **2005**, *152*, A396.
- [109] P. Albertus, S. Babinec, S. Litzelman, A. Newman, *Nat. Energy* **2017**, *3*, 16.
- [110] Q. Ma, F. Tietz, *ChemElectroChem* **2020**, *7*, 2693.
- [111] F. P. McGrogan, T. Swamy, S. R. Bishop, E. Eggleton, L. Porz, X. Chen, Y.-M. Chiang, K. J. Van Vliet, *Adv. Energy Mater.* **2017**, *7*, 1602011.
- [112] G. R. Anstis, P. Chantikul, B. R. Lawn, D. B. Marshall, *J. Am. Ceram. Soc.* **1981**, *64*, 533.
- [113] X. Miao, H. Di, X. Ge, D. Zhao, P. Wang, R. Wang, C. Wang, L. Yin, *Energy Storage Mater.* **2020**, *30*, 170.
- [114] Z. Gao, J. Yang, H. Yuan, H. Fu, Y. Li, Y. Li, T. Ferber, C. Guhl, H. Sun, W. Jaegermann, R. Hausbrand, Y. Huang, *Chem. Mater.* **2020**, *32*, 3970.
- [115] Y. Kim, J. Jung, H. Yu, G. T. Kim, D. Jeong, D. Bresser, S. J. Kang, Y. Kim, S. Passerini, *Adv. Funct. Mater.* **2020**, *30*, 2001249.
- [116] W. Zhou, Y. Li, S. Xin, J. B. Goodenough, *ACS Cent. Sci.* **2017**, *3*, 52.
- [117] M.-C. Bay, M. Wang, R. Grissa, M. V. F. Heinz, J. Sakamoto, C. Battaglia, *Adv. Energy Mater.* **2020**, *10*, 1902899.
- [118] J. Yang, H. Xu, J. Wu, Z. Gao, F. Hu, Y. Wei, Y. Li, D. Liu, Z. Li, Y. Huang, *Small Methods* **2021**, *5*, 2100339.
- [119] H. Fu, Q. Yin, Y. Huang, H. Sun, Y. Chen, R. Zhang, Q. Yu, L. Gu, J. Duan, W. Luo, *ACS Mater. Lett.* **2020**, *2*, 127.
- [120] J. Yu, Y. S. Hu, F. Pan, Z. Zhang, Q. Wang, H. Li, X. Huang, L. Chen, *Nat. Commun.* **2017**, *8*, 14629.
- [121] R. J. Y. Park, C. M. Eschler, C. D. Fincher, A. F. Badel, P. Guan, M. Pharr, B. W. Sheldon, W. C. Carter, V. Viswanathan, Y.-M. Chiang, *Nat. Energy* **2021**, *6*, 314.
- [122] X. Guo, J. Bae, Y. Ding, X. Zhang, G. Yu, *Adv. Funct. Mater.* **2021**, *31*, 2010863.
- [123] Y. Li, H. Wang, W. Yuan, Y. Luo, J. Tu, L. Zhang, J. Shu, *Energy Storage Mater.* **2021**, *42*, 268.
- [124] A. Yang, R. Ye, X. Li, Q. Lu, H. Song, D. Grüner, Q. Ma, F. Tietz, D. Fattakhova-Rohlfing, O. Guillon, *Chem. Eng. J.* **2022**, *435*, 134774.



Qiongqiong Lu is currently a postdoc at the Leibniz Institute for Solid State and Materials Research (IFW) Dresden, Germany. He received his Ph.D. degree from Technische Universität Dresden in 2022 and his M.Sc. degree from Nankai University in 2017. His research focuses on metal anode stabilization and functional materials for batteries.



Aikai Yang received his B.S. and M.S. degrees from Qingdao University (China) and Nankai University (China) in 2016 and 2019, respectively. He then moved to Forschungszentrum Jülich and RWTH Aachen University (Germany) to pursue his Ph.D. degree to date. His current research interests focus on oxide-based ionic conductors for energy storage and all-solid-state batteries design.



Ahmad Omar obtained his bachelor's and master's degrees in metallurgical and materials engineering in 2011 (dual degree program) from Indian Institute of Technology Madras, India. He obtained a Ph.D. degree in physics in 2016 from Technische Universität Dresden, Germany. His doctoral research, undertaken at IFW Dresden, focused on material design and crystal growth for spintronics as well as advanced structural characterization using synchrotron and neutrons facilities. Since 2016, his postdoctoral research at IFW Dresden focuses on operando studies on silicon anodes and oxide cathodes, as well as development of novel materials for batteries and supercapacitors.



Qianli Ma obtained B.S. and Ph.D. degrees at the University of Science and Technology of China, majored in materials science. From 2007 to present, he is working in Forschungszentrum Jülich, IEK-1, Germany, first as postdoc, then as senior scientist, and now as tenure scientist. He specializes in development of nonmetallic inorganic materials. He has detailed researching experiences on the relationships between processing, microstructure and properties, and is especially familiar with R & D of fuel cells and solid-state batteries.



Frank Tietz received his Ph.D. degree in solid-state chemistry from the University of Hanover (Germany). After a Humboldt fellowship at the University of Trento (Italy), he joined Forschungszentrum Jülich (Germany) in 1995. He has worked on a wide variety of ceramic materials at both fundamental and technology development level, including superconductors, cationic and anionic conductors, mixed ionic–electronic conductors as well as ceramic/metal composite materials. Initially working on high-temperature materials for solid oxide fuel cell development and thermal barrier coatings, his current work focuses on new electroceramic materials for different types of solid-state batteries.



Olivier Guillon is materials scientist and became director at the Institute of Energy and Climate Research – Materials Synthesis and Processing (IEK-1, Forschungszentrum Jülich) and professor at the RWTH Aachen University in 2014. He is coordinating the platform “Oxides” in the BMBF-funded competence cluster for solid-state batteries Festbatt and the spokesperson of the research program “Materials and Technologies for the Energy Transition” within the Helmholtz Association. He works on ceramic materials and components for solid-state batteries, solid oxide fuel and electrolysis cells, gas separation membranes, and high-temperature applications. He has published more than 250 articles in international referred journals and is, among others, member of the World Academy of Ceramics.



Daria Mikhailova has obtained a diploma in chemistry in 1996 and a Ph.D. degree in chemistry in 2000 at the Moscow State University, Russia. From 2005 to 2010, she did a postdoctoral work at the Technical University of Darmstadt, Germany. From 2011 to 2017, she worked as a senior scientist at the Max Planck Institute of Chemical Physics of Solids in Dresden, Germany, and at the Karlsruhe Institute for Technology, Germany. From 2017, she is working at the Leibniz Institute for Solid State and Materials Research in Dresden, Germany, in the electrochemical energy storage group, and from 2018 she is the head of the group. Her research focuses on development of metal-ion batteries and supercapacitors including all cell components as cathodes, anodes, binder, and electrolytes.